

# The application of multifactorial cluster analysis in the staging of plaques in early multiple sclerosis

## Identification and characterization of the primary demyelinating lesion

F. W. Gay,<sup>1</sup> T. J. Drye,<sup>2</sup> G. W. A. Dick<sup>1</sup> and M. M. Esiri<sup>3</sup>

Departments of <sup>1</sup>Biomedical Science and <sup>2</sup>Mathematics, Anglia Polytechnic University, Cambridge, and the <sup>3</sup>Department of Clinical Neurology and Neuropathology, Radcliffe Infirmary, Oxford, UK

Correspondence to: Dr F. W. Gay, Department of Biomedical Science, Anglia Polytechnic University, Cambridge CB1 1PT, UK

### Summary

Tissues from 13 exceptionally early cases of multiple sclerosis were studied to identify and characterize the primary demyelinating lesion, using a variety of histological and immunocytochemical methods. Multifactorial cluster analysis identified five significantly distinct lesion groups, which showed histological progression from simple microglial lesions, predominating in tissues from the earliest cases, to complex hypercellular fully demyelinated plaques, chiefly associated with cases of intermediate duration. Quiescent lesions showing evidence of remyelination were found at all stages of the disease studied, but hypocellular inactive plaques, were associated with older cases. Evidence is presented that initial demyelination is effected by activated

resident microglia. Undegraded myelin is initially enveloped by membranes bearing fixed complexes of immunoglobulin and complement. In contrast with perivenous encephalomyelitis, in which demyelination was dominated by T-cell infiltration, multiple sclerosis lesions of comparable duration and maturity exhibited humoral immune reactions. Parenchymal CD4<sup>+</sup> T-cell infiltration developed in association with subsequent plaque maturation. These results emphasize the need for lesion staging when multiple sclerosis tissues are being used in the investigation of pathogenic mechanisms, and suggest that further analysis of the oligoclonal B-cell response may be productive in the search for primary provoking antigens.

**Keywords:** primary multiple sclerosis plaque; cluster analysis

**Abbreviations:** AEC = 3-amino-9-ethylcarbazole in *N*, *N*-dimethylformamide and 0.3% hydrogen peroxide; AWE = approximate weight of evidence; EAE = experimental allergic encephalomyelitis; FITC = fluorescein isothiocyanate; H&E = haematoxylin and eosin; HLA-DR = human lymphocyte antigen-DR; HRP = horseradish peroxidase; LFB = Luxol fast blue; MHC = major histocompatibility complex; NBT = nitro-blue tetrazolium; ORO = Oil Red O; *R* = Rand ratio; SSPE = subacute sclerosing panencephalitis; TRITC = tetra-rhodamine isothiocyanate

### Introduction

A diversity of pathological processes elicit cellular and humoral immune responses within the CNS, usually though not invariably, initiating clinically important tissue damage. In the primary demyelinating diseases such as multiple sclerosis and perivenous (post-infectious) encephalomyelitis, the myelin sheath is believed, by analogy with experimental allergic encephalomyelitis (EAE), to be the target of CD4<sup>+</sup> T-cell mediated damage (Ransohoff *et al.*, 1994; Utz and McFarland, 1994) and lymphocytic infiltration has been proposed as the primary event in the genesis of the multiple

sclerosis plaque (Hafler and Weiner, 1989). However, it has not been possible to provide direct evidence of a specific autoimmune T-cell target and the mechanism of demyelination in multiple sclerosis remains uncertain. A majority of studies have shown disconcertingly heterogeneous T- and B-cell responses (Pelfrey *et al.*, 1996), and the observed diversity of T- and B-cell reactivity to myelin and to other antigens, may reflect secondary processes of non specific sensitization or immune activation (Esiri and Gay, 1997).

Primary pathogenic processes are most likely to be

recognized in initial lesions but the primary demyelinating lesion in multiple sclerosis has not been identified with any certainty and it is probable that the inflammatory processes observed in established plaques inflict myelin sheath damage and, later, axonal damage, by different mechanisms. This view is strongly supported in a recent review by Lucchinetti *et al.* (1996), in which they also provide new data suggesting considerable heterogeneity of mechanisms of myelin and oligodendrocyte destruction in active lesions.

Clues to the nature of an inciting stimulus and to the pathogenesis of tissue damage may be obtained from an analysis of the immune response generated, be it cell-mediated or humoral in emphasis, and attempts have been made in recent years to exploit immunocytochemical techniques to characterize various inflammatory and demyelinating conditions of the CNS according to their immunological profiles. Of particular interest has been the use of monoclonal antibodies that identify subpopulations of lymphocytes, macrophages and immunologically significant surface molecules such as class I and class II major histocompatibility complex (MHC) (McCallum *et al.*, 1987; Fabry *et al.*, 1994; Esiri and Gay, 1997). Other studies have concentrated on the localization of membrane-bound or secreted proteins such as immunoglobulins, complement, adhesion molecules and cytokines (Esiri, 1980; Compston *et al.*, 1989; Brosnan *et al.*, 1995; Woodrooffe, 1995).

No specific pattern of inflammation has been recognized in these studies and some confusing discrepancies between research groups have been attributed to the lack of an accepted method of lesion staging, and also to differences in immunohistological techniques between laboratories (Raine, 1994; Utz and McFarland, 1994).

An additional problem is the evidence that the tissues represented in CNS sections comprise a number of separate compartments. Recent evidence supports Dawson's original contention (1916) that the perivascular Virchow–Robin spaces represent the lymphatic system of the CNS where, relatively isolated from brain parenchyma, full-blown immunological responses may be generated in communication with the regional cervical and nasopharyngeal lymph nodes (Prineas, 1979; Rennels *et al.*, 1985; Esiri and Gay, 1990; Zhang *et al.*, 1992). The Virchow–Robin space, separated from the CNS parenchyma by the glia limitans, needs to be taken into account in describing and quantifying immune activity ostensibly 'within' lesions. Perivascular cuffs of inflammatory cells are frequently found in multiple sclerosis tissues in the absence of perivascular demyelination (Adams, 1977).

We report here a quantitative histological and immunocytochemical study of 155 lesions from 13 exceptionally early cases of multiple sclerosis (Cases 1–13, Appendix 1). These rare cases were selected to increase the probability of encountering initial lesions and their immediate derivatives, relatively uncomplicated by secondary events. Parallel studies were carried out on other demyelinating and inflammatory conditions of comparable clinical duration and on various control tissues (Cases 14–26, Appendix 1). Paraffin embedded

and frozen tissues were analysed in parallel using a variety of histological and immunocytochemical methods to provide quantitative data for multifactorial cluster analysis, which was then used to assist in the definition of significant stages in lesion maturation. Lesions identified and classified by these methods were studied using additional immunocytochemical techniques to characterize the cellular and immune reactions within CNS tissue compartments and to describe the immune events associated with the initiation of myelin sheath damage.

## Methods

### *Histological and immunocytochemical methods*

Clinical details of the autopsy tissues studied are given in Appendix 1. Paraffin sections stained with haematoxylin and eosin (H&E) and with Luxol fast blue (LFB), were used to survey the available tissue blocks. Initially, 92 distinct lesions ('first series') were identified in the 13 acute and sub-acute multiple sclerosis cases. Cryostat sections were stained with Oil Red O (ORO) to assess the extent of myelin phagocytosis and esterification, and with antibodies selected from the panel detailed in Appendix 2.

Total cell counts (cell nuclei) and 'giant' astrocyte counts were made using a  $\times 20$  objective and a standard square grid, within defined plaque zones, namely, perivascular (central), parenchymal (main body of the plaque) and plaque border, and also in surrounding non-plaque tissue. A minimum of 10 grids were used in each area and the mean count calculated.

Quantitative assessments of myelin degradation within these zones were based on the density of LFB<sup>+</sup> and ORO<sup>+</sup> inclusions in macrophages, Grades from 1 to 4+. Similar assessments were made on the density of collagen Type IV fragments in the parenchyma, reflecting lesion maturation (Gay and Esiri, 1991), and on the degree of disruption of the blood–brain barrier, by quantifying the perivascular leakage of fibrinogen, after staining with the appropriate antibodies.

In a previous communication, some acute multiple sclerosis plaques were shown to contain complexes of C3d and IgG co-locating on the membranes of microglial macrophages and on material within the Virchow–Robin spaces (Gay and Esiri, 1991; Esiri and Gay, 1997). To assess these findings further in relation to plaque maturity, cryostat sections were double labelled for C3d–fluorescein isothiocyanate (FITC) and human IgG–tetra-rhodamine isothiocyanate (TRITC) after washing the sections for 2 h with Tris buffer, pH 4.5, to remove unfixed immunoglobulin (Pambakian and Poston, 1987). Serial or adjacent sections were also stained for the C9 neoantigen.

### *Statistical analysis*

Examples of lesion profiles constructed from the quantitative data are shown in Figs 1–3. The data collected from the 92 lesions identified in the initial study, were pooled and subjected to Gaussian cluster analysis with *S\** matrix methods

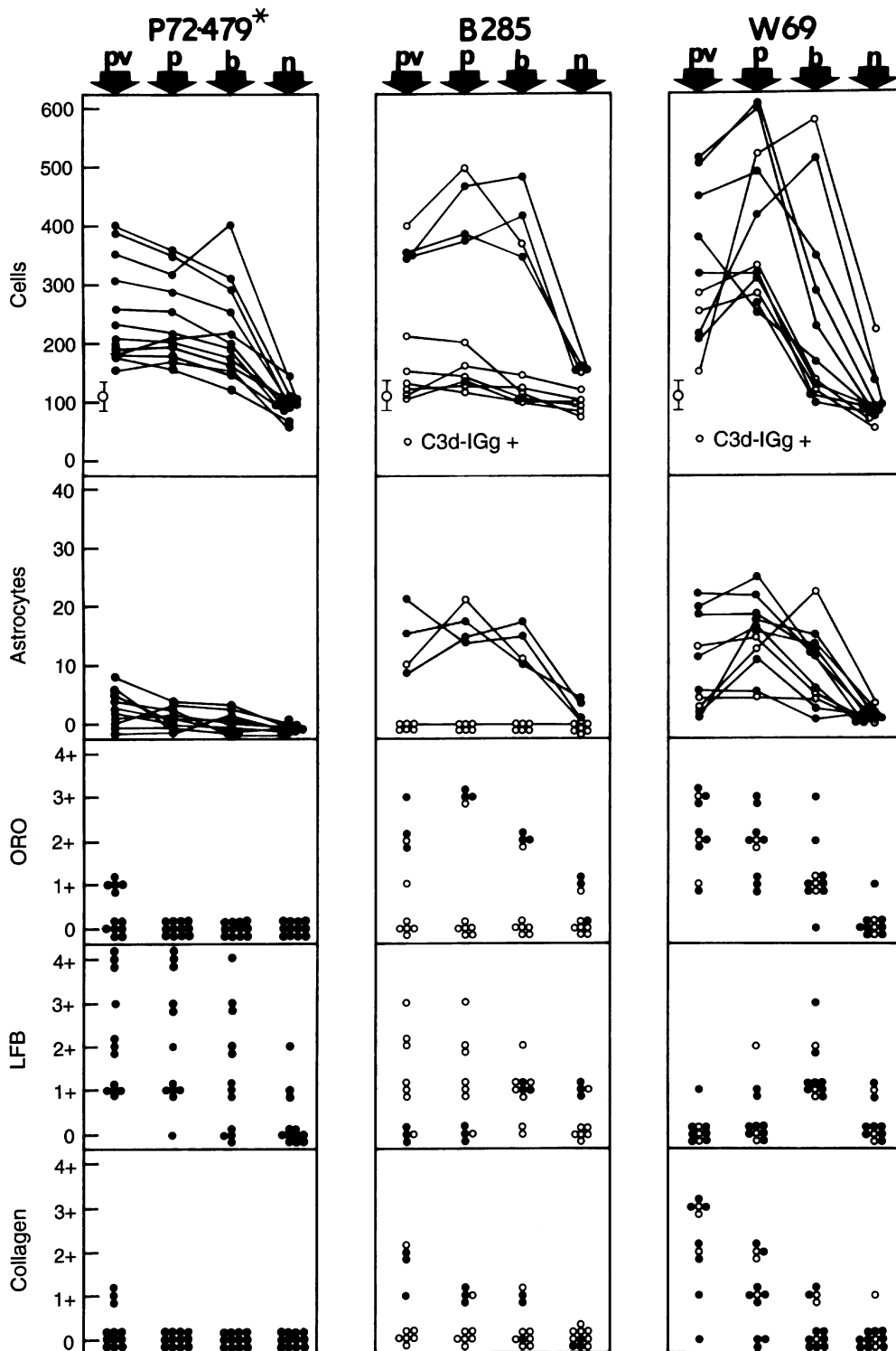


Fig. 1

**Figs 1–3** Lesion profiles of acute and subacute multiple sclerosis cases of increasing clinical duration, and of chronic inflammation controls (B9055 and B8946) (*see* Appendix 1 for clinical data). Total cell counts (nuclei) per standard grid (SD bar concerns normal white matter), with giant astrocyte counts, and graded assessments (Grades 1 to 4+) of oil red O (ORO) and luxol fast blue (LFB) positive inclusions in macrophages, and collagen IV fragments (parenchymal fibrinogen not included). The lesion profiles were constructed from the histological data in four locations; perivascular or central (pv), main plaque parenchyma (p), plaque border (b), and periplaque normal tissue (n). In Fig. 1 open circles represent C3d/IgG<sup>+</sup> lesions, and in Fig. 3 open triangles represent lesions with evidence of remyelination. \*P72.479 (Fig. 1) and \*B670 (Fig. 3), cryostats were not available for IgG/C3d assessment.

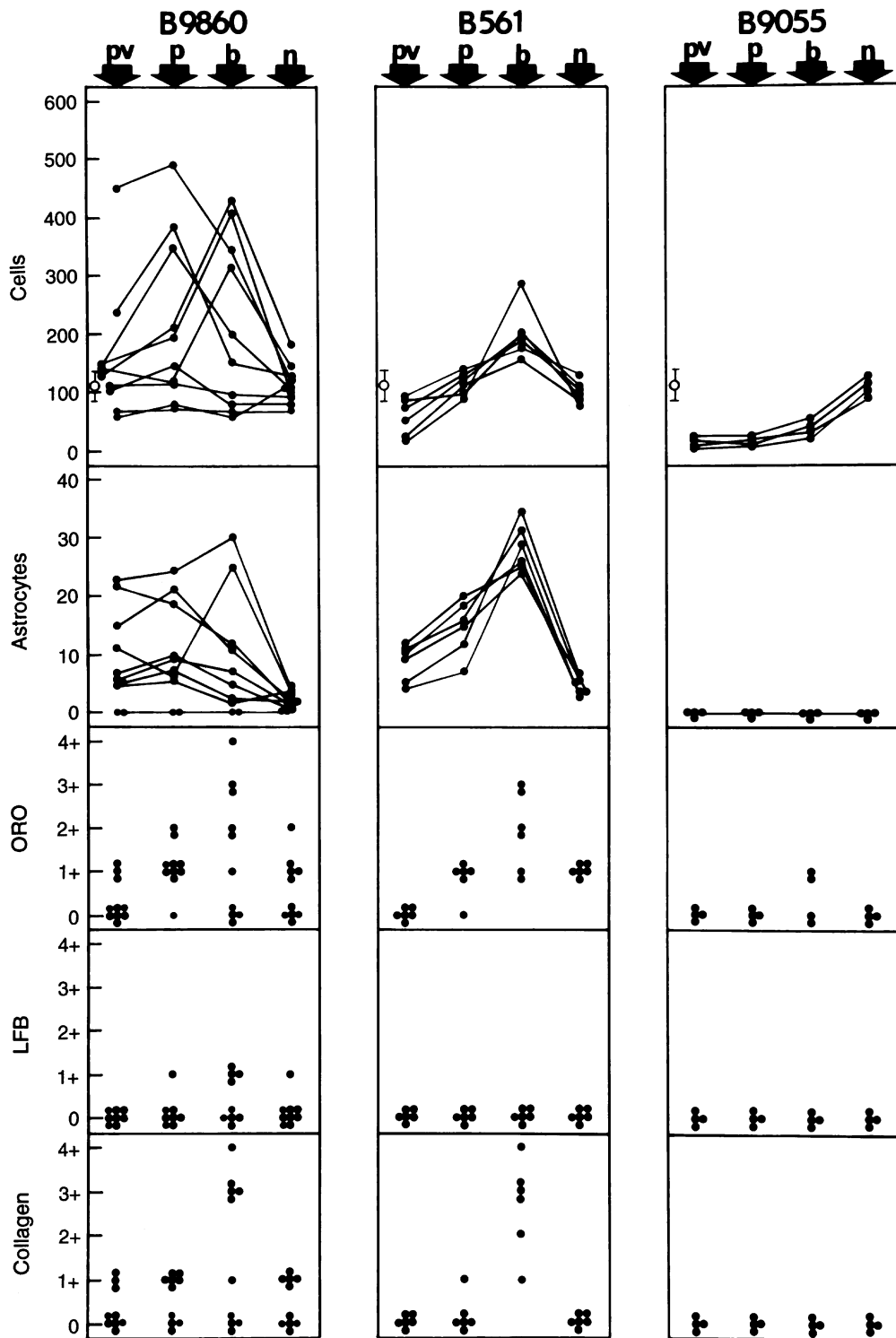


Fig. 2

(Banfield and Raftery, 1993). This was implemented by S-PLUS version 3.1 statistical software (Statistical Sciences, S-PLUS for windows, Seattle: Stat Sci, Mathsoft, 1994). The analysis was carried out using the seven variables detailed above, namely, total cell counts, giant astrocyte counts, ORO<sup>+</sup> inclusions in macrophages, collagen IV fragmentation,

parenchymal fibrinogen, LFB<sup>+</sup> inclusions in macrophages and the presence of C3d/IgG complexes. Where data related to the four plaque zones studied (see Figs 1–3), mean values were used. The best discrimination was found by using a logarithmic transformation, which can account for the error structure normally associated with counted or concentration

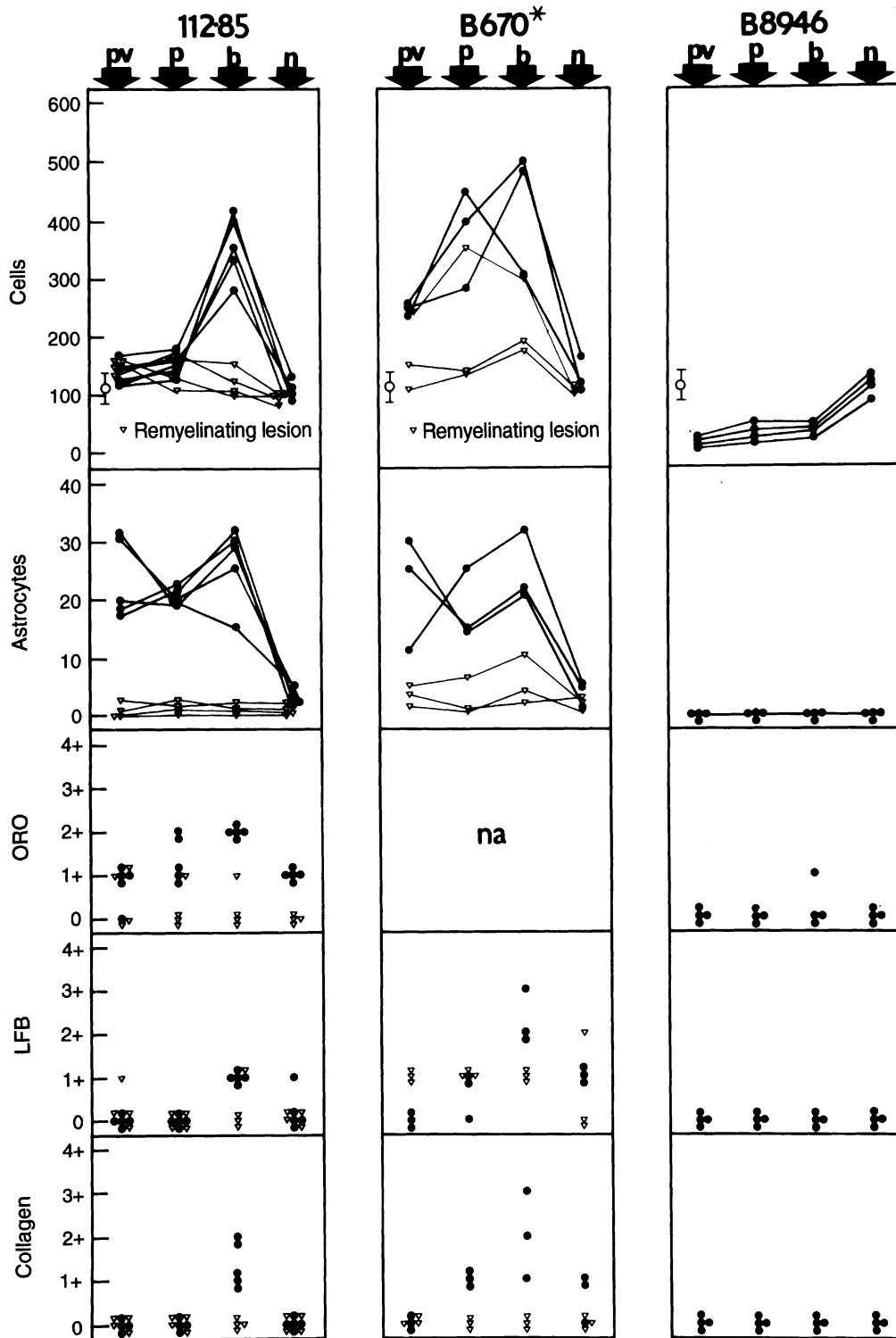


Fig. 3

data of this type. The 'approximate weight of evidence statistic' (AWE) peaked at three clusters and remained positive up to five (*see* empirical mean values of the AWE in Table 1). As recommended by Banfield and Raftery (1993), the analysis focused on the largest number of plausible

clusters which submit to a parsimonious interpretation. These data were plotted with each of the axes as a linear combination of standardized variables. The statistical techniques employed avoided any interpretative imposition of axes as the initial choice was guided by principal component analysis. The

axes chosen were those which described the largest amount of variation within the data, reflecting the plane of the most dominant structures. In order to obtain the primary and secondary axes described below, we rotated the plane slightly to aid interpretation. When the primary axis consisted of an equally weighted linear combination of the standardized LFB data combined with the C3d/IgG results and the secondary axis was a combination of the remaining data, i.e. total cellularity, giant astrocyte counts, ORO<sup>+</sup> inclusions in macrophages, fibrinogen leakage, and collagen Type IV fragments, the structures shown in Fig. 4 were obtained. Further cluster resolution was obtained by applying a tertiary axis consisting of cellular values plus astrocyte values minus fibrinogen and ORO data combined. Figure 5 shows the structures obtained in this analysis. The fifth cluster was identified mainly with

**Table 1** The 'approximate weight of evidence' (AWE) statistic

| No. of groups | Empirical mean AWE | Empirical SEM AWE | Original measured AWE |
|---------------|--------------------|-------------------|-----------------------|
| 2             | 113                | 90                | 80                    |
| 3             | 130                | 132               | 91                    |
| 4             | 99                 | 139               | 40                    |
| 5             | 47                 | 142               | -26                   |
| 6             | -15                | 142               | -106                  |

The 'approximate weight of evidence' (AWE) statistic for the  $S^*$  classification, with estimated mean and standard errors (SEM) derived from 1000 parametric boot-strapped samples.

the lesions showing histological evidence of remyelination (Type IV). The presence of this clustering structure was confirmed in the additional clustering methods employed (see below), where the greatest divergence of classifications was around the membership of the Type IV cluster.

Frozen tissue was not available in all cases (see Appendix 1). To test the comparability of clusters obtained using data exclusively derived from cryostats, with those obtained from paraffin sections (where ORO and C3d/IgG data were not available), both sets were resampled 1000 times using a multinormal parametric bootstrap to derive empirical 95% confidence regions for cluster means. The cluster means were then displayed in a variable plane which defines the standardized lesion characteristics, as seen in Figs 4 and 5. From the cluster means confidence regions were estimated using empirical contouring. These are displayed for the frozen lesions in Fig. 6 and, for comparison, an identical analysis for the paraffin data is shown in Fig. 7. It may be seen that clusters defined in frozen sections alone significantly overlay those defined using data derived from paraffin sections.

The structures obtained were consistent across a variety of standardization methods including Z-standardization ranking and log transformation and they were confirmed as a 'near optimal' view using principal component analysis.

In order to demonstrate the reliability of the classification scheme produced by the  $S^*$  method, other clustering techniques, available within the S-PLUS software, were applied. Each classification was compared using the Rand ratio ( $R$ )

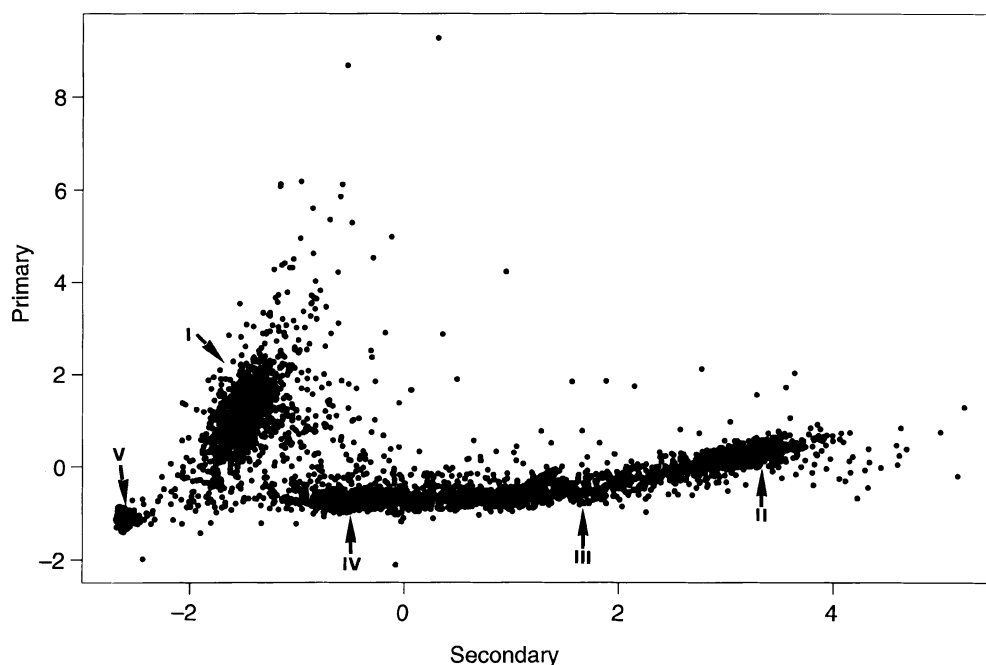


**Fig. 4** Cluster analysis of multiple sclerosis lesions ( $n = 92$ ). The points plotted are the cluster centres of each of the 1000 resamples. The primary axis consists of an equally weighted linear combination of the standardized LFB<sup>+</sup> inclusions in macrophages plus C3d/IgG data (positive or negative). The secondary axis is a combination of total cellularity, ORO<sup>+</sup> inclusions in macrophages, parenchymal fibrinogen and collagen IV fragments. The locations of lesion Types I–V are indicated (for histological characteristics see Table 3).

(Rand, 1971; Fowlkes and Mallows, 1983). The ratio  $R$  is the percentage of pairs of data points in a sample which are similarly dealt with in each classification, i.e. those pairs in the same grouping in both classifications and those in different groupings in both classifications. Table 2 details the  $R$  ratio between each classification available, and the  $S^*$  classification used [see Banfield and Raftery (1993), the S-PLUS manual and Venables and Ripley (1994) for a specification of each method]. The table demonstrates the stability of the classification scheme. For comparison, a random partition into five groups has an  $R$  of 64%. The model-based classification schemes similar in nature to the  $S^*$  method, yield high  $R$  ( $>80\%$ ). The dense type methods of classification have values  $\sim 70\%$ . Not surprisingly, the single-link scheme is most different. The discrepancy is an indication of the type of partitioning present. As would be expected there is an underlying gradual progression between plaque types with allowable intermediate positions. This is consistent with the hypothesis that the lesion variants lying between the major plaque types are transitional, and the classifications given indicate the characteristics through which the lesions progress on the way to greater maturity. Data of this type are less susceptible to single link type methods which allow the growth of long 'strings' in the data, irrespective of the local identity of the data points (Everitt, 1993). This means that a cluster is only defined if all data points within the cluster are closer to each other than to any data point outside the group, a situation unlikely to occur in the associated multiple sclerosis data due to the transitional position of some plaques.

To allow further confirmation of the presence of structure within the plaque profiles, simulation studies were conducted.

Simulations generated four random planes within the data space, constrained only to partition at least one data point. Once generated a hierarchical partition was implemented to optimize the entropy of the partition produced (Venables and Ripley, 1994). This non-parametric simulation explores all possible classification schemes based on linear partitions of the data. As a result of the simulation, an empirical distribution of  $R$  was generated, firstly by comparing two randomly generated classification schemes to give  $R$  (%) =  $(65.38 \pm 0.50)$  based on 1000 simulation runs. The uncertainty spans the 95% confidence interval assuming that the asymptotic behaviour of  $R$  is normal. This is significantly  $>64\%$  suggesting the presence of structure within the data. Additional evidence for the structure derived from the  $S^*$  method is given by a comparison of  $R$  for random permutations of the  $S^*$  classification. These simulations merely preserve the same size of the clusters irrespective of any other information, the average  $R$  after 1000 simulations was  $R$  (%) =  $(65.45 \pm 0.08)$ , consistent with the value obtained for the random classifications indicating that the structure has a similar group size distribution. Further simulations compared the  $S^*$  classification used with an additional 1000 random classifications and gave  $R$  (%) =  $(66.43 \pm 0.42)$ , suggesting that the  $S^*$  classification is somewhat better at describing the classification structure than any randomly chosen scheme.

Closer examination of the different classifications pointed to the Type IV (remyelinating) group as the least well defined, followed by the two intermediate groupings, II (secondary) and III (border active). The most stable classifications were Group I (primary) and Group V (chronic/inactive).

A further 63 lesions ('second series') were later identified

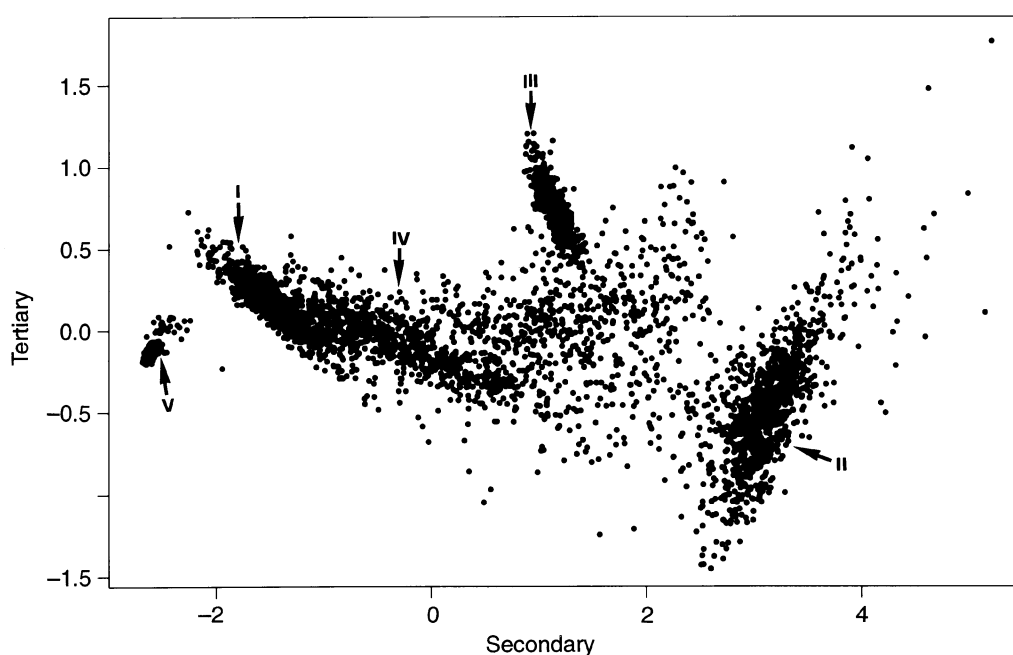


**Fig. 5** Cluster resolution of lesions, Types I-V, using a tertiary axis consisting of total cellular values plus astrocyte values minus fibrinogen and ORO data combined.

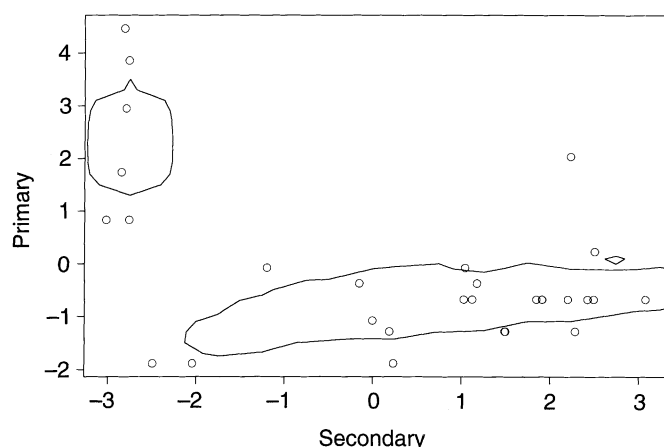


**Fig. 6** Resampled cluster analysis of data from cryostats. Approximate 95% confidence regions for the cluster means and the original data points are shown.

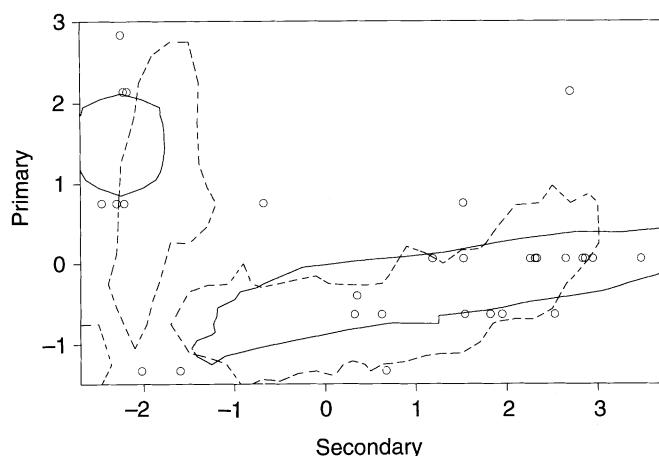


**Fig. 7** Comparability of clustering between data derived from cryostats and from paraffin sections. Combined resampled cluster analysis of data from frozen (continuous line) and paraffin embedded tissues (broken line), the latter lacking ORO and C3d/IgG data.

**Table 2** A comparison of the  $S^*$  classification with other classification methods

| Clustering method compared with $S^*$ | Rand ratio $R$ (%) | Jack-knife SEM (%) | Jack-knife bias (%) |
|---------------------------------------|--------------------|--------------------|---------------------|
| $S$                                   | 82.0               | 3.0                | 0.4                 |
| Spherical                             | 80.9               | 3.1                | 1.1                 |
| Trace                                 | 80.3               | 3.5                | 2.7                 |
| Unconstrained                         | 80.9               | 3.1                | 1.1                 |
| Determinant                           | 83.9               | 2.9                | -2.1                |
| Centroid                              | 76.8               | 1.8                | 0.1                 |
| Weighted average link                 | 72.9               | 3.6                | 2.9                 |
| Group average link                    | 74.0               | 3.1                | 1.9                 |
| Complete link                         | 75.8               | 1.9                | 0.9                 |
| Single link                           | 47.8               | 4.4                | 3.8                 |

A comparison of the  $S^*$  classification with other classification methods available within the 'S-PLUS' software. The table shows the observed Rand ratio ( $R$ ) with a jack-knife estimate of standard error and bias. The jack-knife estimates are obtained by repeating the analysis, eliminating each data point in turn.

in tissue blocks from the 13 cases. These were studied and classified using the histological methods described above, but excluding quantitative assessments.

### Concurrent single field analysis of lymphocytes

Using the standard square grid and a  $\times 20$  objective, counts of  $CD4^+$ ,  $CD8^+$  and  $\gamma\delta$  T-cells and plasma cells were made on immunostained 5  $\mu$ m cryostat sections. Serial sections were cut in triplicate, mounted on poly-L-lysine coated slides and fixed in acetone for 6 min. The first section was immunostained for plasma cells using a cocktail of rabbit  $F(ab')_2$  anti-human IgG, IgA and IgM. Horseradish peroxidase (HRP) labelled affinity-purified swine anti-rabbit, as second antibody, was followed by colour development in 3-amino-9-ethylcarbazole in  $N, N$ -dimethylformamide and 0.3% hydrogen peroxide in water (AEC).

The second section was treated with  $\gamma\delta$  antibody 5A6.E9, followed by biotinylated anti-mouse antibody and, finally, HRP-labelled streptavidin. Colour development was in AEC.

The third section was treated with an equal mixture of biotinylated anti- $CD4^+$  (MT.310, IgG1, kappa) and anti- $CD8^+$  (RFT-8, IgM). Second antibodies were streptavidin-HRP and phosphatase-labelled goat anti-mouse IgM.  $CD4^+$  cells were detected with the AEC reagent. After washing in Tris-buffered saline for  $\geq 6$  h,  $CD8^+$  cells were detected using the nitro-blue tetrazolium (NBT) reaction. After washing in water for a minimum of 6 h, sections were mounted in 'Glycergel' (Dako).  $CD4^+$  and  $CD8^+$  cells were counted simultaneously in meningeal tissue, perivascular (Virchow-Robin) spaces, in lesion parenchyma and at the lesion edge using the standard grid, the edge being conveniently detected using polarized light (Adams, 1989). The same locations identified in the serial sections were counted for  $\gamma\delta$  T-cells and for plasma cells. A minimum of 10 triplicate sections were counted for each lesion studied.

A variant of this method was used in selected cases to increase sensitivity in the detection of  $CD4^+$  cells which, despite employment of a variety of monoclonal antibodies, singly and as cocktails, tended to show weak reactivity which could be obscured by the counter-staining effect of NBT. After  $CD4^+$  development with AEC and washing in Tris-buffered saline,  $CD4^+$  cells were counted in defined zones, as described above, in the wet preparation. Development in NBT, washing and mounting were then carried out, and  $CD8^+$  cells were counted in the same defined fields (see Fig. 13B and B'). Cell counts were recorded in different tissue zones, as described above.

Reagent and observer controls for each run involved normal human Ficoll purified peripheral blood leucocytes double labelled for  $CD4^+$  and  $CD8^+$  cells. The  $CD4^+/CD8^+$  ratio in control experiments was  $2.15 \pm 0.11$  SEM (Fig. 13A'). Staining of  $\gamma\delta$  T-cells was controlled using peripheral leucocytes from a rheumatoid patient ( $8\% \pm 1.6$  SEM).

**Table 3** Analysis of histological and immunocytochemical characteristics of multiple sclerosis lesions

|                                       | Type I     | Type II    | Type III      | Type IV       | Type V           |
|---------------------------------------|------------|------------|---------------|---------------|------------------|
| Proposed designation                  | Primary    | Secondary  | Border active | Remyelinating | Chronic/inactive |
| First series ( <i>n</i> = 92)         | 24 (26.0%) | 16 (17.3%) | 40 (43.4%)    | 9 (9.7%)      | 3 (3.2%)         |
| Second series ( <i>n</i> = 63)        | 23 (36.0%) | 7 (11.1%)  | 21 (33.3%)    | 8 (12.6%)     | 4 (6.3%)         |
| Luxol fast blue inclusions            | +          | +          | -, (+)e       | +             | -                |
| Oil red O inclusions                  | -, (+)     | ++         | (+), ++e      | Not done      | -                |
| C3d/IgG complexes                     | ++         | (+)        | -             | Not done      | -                |
| Perivascular fibrinogen               | -, (+)     | ++         | (+), +e       | (+)           | -                |
| Collagen IV fragments                 | -          | ++         | +, ++e        | -             | -                |
| Giant astrocytes                      | -, (+)     | ++         | +++e          | (+)           | -                |
| Oligodendrocytes                      | +          | -, (++e)   | -             | + / ++        | -                |
| HLA-DR <sup>+</sup> microglia         | +          | (+), +e    | -, +e         | Not done      | -                |
| EBM11/HAM56/Y1/83A <sup>+</sup> cells | (+)        | ++         | +, +++e       | (+)           | (+)              |
| RFD7 <sup>+</sup> cells               | -, (+)     | +          | ++            | Not done      | (+)              |
| Parenchymal CD4 <sup>+</sup> T cells  | (+)        | +          | +             | Not done      | -                |
| Parenchymal CD8 <sup>+</sup> T cells  | +          | +, ++e     | +e            | Not done      | -                |
| Parenchymal $\gamma\delta$ T cells    | -          | +          | +             | Not done      | -                |

Histological and immunocytochemical characteristics of multiple sclerosis lesions (Cases 1–13) grouped I–V by multifactorial cluster analysis (*n* = 92, first series), and subsequently by qualitative assessment (*n* = 63, second series). e = relating particularly to lesion edge. (+) = occasionally, or weakly positive.

## Results

### Quantitative analysis of lesions, 'first series' (*n* = 92)

The five significantly distinct data clusters indicated by the application of the 'approximate weight of evidence statistic' were resolved using Gaussian cluster analysis, and were designated Types I–V according to their histological and immunocytochemical characteristics. These are summarized in Table 3. The analysis to test the comparability of clusters detected in cryostat and paraffin sections, showed that strikingly similar results are obtained (Figs 6 and 7).

### Qualitative analysis, 'second series' (*n* = 63)

Lesions were categorized according to the histological and immunocytochemical characteristics identified in the first series. The proportion of lesions falling into Categories I–V closely resembled the distribution of lesion types in the first series (see Table 3).

### Type I lesions

The data cluster designated Type I (Fig. 4) was largely defined by the combination of LFB<sup>+</sup> inclusions within microglial cells and C3d/IgG<sup>+</sup> complexes on microglial cell membranes. These lesions were recorded 30.3% overall but were the predominating type (60.6%) in the tissues obtained from the earliest cases, with a history of a terminal attack  $\leq 5$  weeks (see Fig. 8).

Type I lesions predominated in Cases P72.479 and B285 (2 weeks and 1 week duration of terminal illness, respectively) and the data profiles of lesions found in these cases (Fig. 1), unexpectedly showed that total cellularity may be within

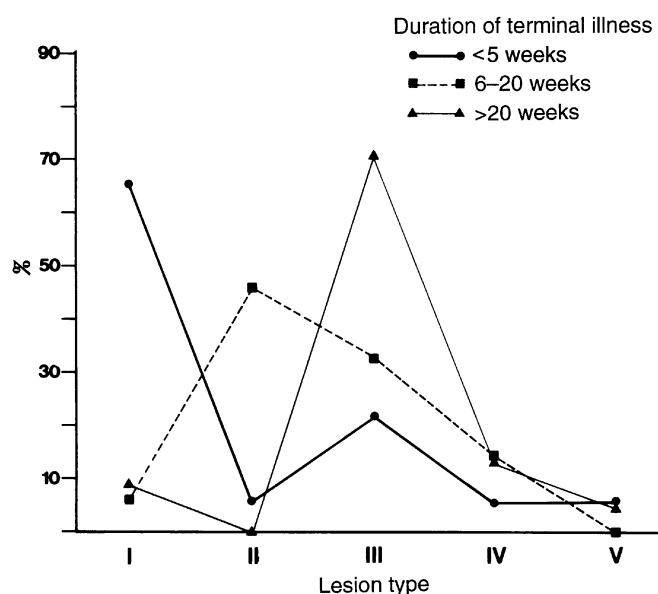


**Fig. 8** Percentage distribution of multiple sclerosis lesion Types I–V (*n* = 155) according to the duration of the terminal demyelinating illness in weeks ( $\chi^2 = 81.88$ , d.f. = 8; likelihood ratio test = 95.14,  $P < 0.0001$ ).

normal limits (B285), or only moderately elevated (P72.479). It can also be seen that lesions containing C3d/IgG complexes (B285) had the lowest cellularity, least evidence of astrocytosis, and they tended to be ORO and collagen Type IV negative, but LFB<sup>+</sup>, in all zones. A further unexpected feature of these lesions was that parenchymal reactions for fibrinogen, indicating a breach in the blood–brain barrier, were not usually detected. Low levels of perivascular fibrinogen (grades from 1 to 2+) were found in those Type I lesions

showing greatest myelin disruption and highest total cell counts (e.g. Fig. 9B).

Focal Type I lesions with demyelination grades from 1 to 2+ (Fig. 9A) consisted of groups of microglial macrophages with reactivity for C3d. Examination at high power and using immunofluorescence combined with polarized light, consistently showed that complement was located on cytoplasmic membranes enclosing birefringent myelinic material (Fig. 9A' and inset). The central vessel in these lesions was frequently a capillary or small vein but in some instances the vessel was identified as an artery (Fig. 9A' inset) by the presence of several layers of smooth muscle positive for actin (HHF35<sup>+</sup>). Double labelling of Type I lesions (Fig. 9A) showed reactivity for fibrinogen within the lumen of vessels but rarely in the parenchyma. All the Type I lesions studied contained HLA-DR<sup>+</sup> microglial cells, which were weakly positive for the macrophage monoclonal antibodies EBM 11, Y1.82A and HAM 56, but RFD 7<sup>+</sup> 'foamy' macrophages were very rarely detected.

Transverse sections of cord containing Type I lesions in the dorsal and ventral long tracts, viewed with polarized light, showed Class II, HLA-DR<sup>+</sup>/EBM11<sup>+</sup> microglia, characteristically intercalated between morphologically intact myelin sheaths (Fig. 10A–C). The cytoplasmic membranes of these cells were strongly positive for C3d complement and enclosed birefringent myelinic material. Double labelling for C3d and IgG showed colocalizing complement and immunoglobulin which was not removed by washing sections at pH 7.4 or 4.5 for 6 h prior to staining (Fig. 10D).

Reactions to the activated membrane attack complex C5b–9 were found within and around Type I lesions. Deposits of C5b–9 were found within small vessel walls and especially in the sub-endothelial Virchow–Robin spaces. Other deposits were found in the parenchyma, in a similar distribution to that of C3d/IgG, namely on or within microglial cells closely associated with the surface of apparently intact myelin sheaths (Fig. 10C inset). The overall distribution of C5b–9 in these lesions closely resembled the pattern described by Linington *et al.* (1989) in acute antibody-mediated demyelinating EAE (a detailed analysis will be reported separately).

Type I lesions showing minimal Grade 1+ demyelination (Fig. 10E) could be entirely ORO negative (Fig. 10E'), but strongly reactive for HLA-DR (Fig. 10F) and more significantly, positive with Clone 10 (Fig. 10G) which detects the myelin basic protein epitope 80–89 with a cleavage at amino acids 89–90 (Groom *et al.*, 1985). Areas within these lesions, showing increased myelin disruption, contained groups of microglia with Grade 1 to 2+ ORO<sup>+</sup> inclusions indicating the early establishment of myelin lipid esterification (Fig. 10H). Adjacent areas showed LFB<sup>+</sup> inclusions in microglia.

Type I lesions contained normal oligodendroglia positive for the monoclonal 14E (Newcombe and Cuzner, 1988) and for Clone 10.

No reactivity to complement components C3 or C9, or to IgG, IgM or IgA was detected on the surface of myelin

sheaths, on myelinic debris or on oligodendroglia, and this was confirmed using two- and three-layered peroxidase or phosphatase immunostaining and avidin–biotin amplification.

HLA-DR<sup>+</sup> microglial cells identified in frozen sections of perivenous encephalomyelitis, subacute sclerosing panencephalitis (SSPE) and in gliomas were unreactive for C3d–IgG complexes.

### Lesion Types II–V

The wider scattering of the Type I data cluster seen in Fig. 4 was the result of lesions showing increased overall activity, e.g. Fig. 9B, which shows Grade 2–3+ myelin disruption with raised cellularity and Grade 1+ fibrinogen leakage, undoubtedly representing lesion progression.

The application of a tertiary axis (Fig. 5) resolved five data clusters as predicted by the 'approximate weight of evidence statistic'. The Type II cluster represented a group of lesions predominating (45.2%; Fig. 8) in tissues from cases of intermediate clinical duration, that is, between 6 and 20 weeks. These lesions showed the greatest degree of overall activity, with maximum cellularity, giant astrogliosis and fibrinogen leakage within the central plaque parenchyma (Fig. 11A and B), accompanied by central ORO<sup>+</sup> (Fig. 11C) and LFB<sup>+</sup> inclusions and collagen Type IV fragments (Fig. 11D). Type II profiles are seen in cases B285 and W69 (Fig. 1). The predominating cell type was the EBM 11<sup>+</sup>, Y1.82A<sup>+</sup> and HAM56<sup>+</sup> macrophage containing ORO<sup>+</sup> inclusions. Macrophages with microglial morphology were confined to the edge of these lesions, and the parenchymal macrophage population contained numerous RFD 7<sup>+</sup> 'foamy' cells. HLA-DR and macrophage monoclonal staining, was characteristically intensified when these cells were located within perivascular spaces (Fig. 11B and inset). Oligodendrocytes were not found in the parenchyma of Type II lesions but a small proportion showed increased numbers of oligodendroglia at lesion margins.

Reactions for C3d/IgG complexes were identified in 28.5% of Type II lesions, on microglial membranes at lesion edges and in a single grey matter lesion, within the parenchyma. Although groups of HLA-DR<sup>+</sup>, ORO<sup>+</sup>, RFD7<sup>+</sup> foamy macrophages were usually surrounded by strong perivascular and parenchymal reactions for plasma proteins including fibrinogen, alpha-2 macroglobulin, C1q complement and immunoglobulins, fixed colocalizing IgG and C3d reactions were not detected on the membranes of these cells.

The cluster classified as Type III (Fig. 5) represented lesions predominating (70.2%, Fig. 8) in cases greater than 20 weeks duration. This group was differentiated largely on account of the reduction of activity at the lesion centre and its persistence at the lesion edge. This feature may be seen in the plaque profiles for cases B9860, B561 and 112.85 in Figs 2 and 3. Total and astrocyte hypercellularity at lesion edges was accompanied by a tendency towards central hypocellularity, with low ORO<sup>+</sup>, LFB<sup>+</sup> and collagen IV<sup>+</sup> counts. Parenchymal fibrinogen was reduced overall but when

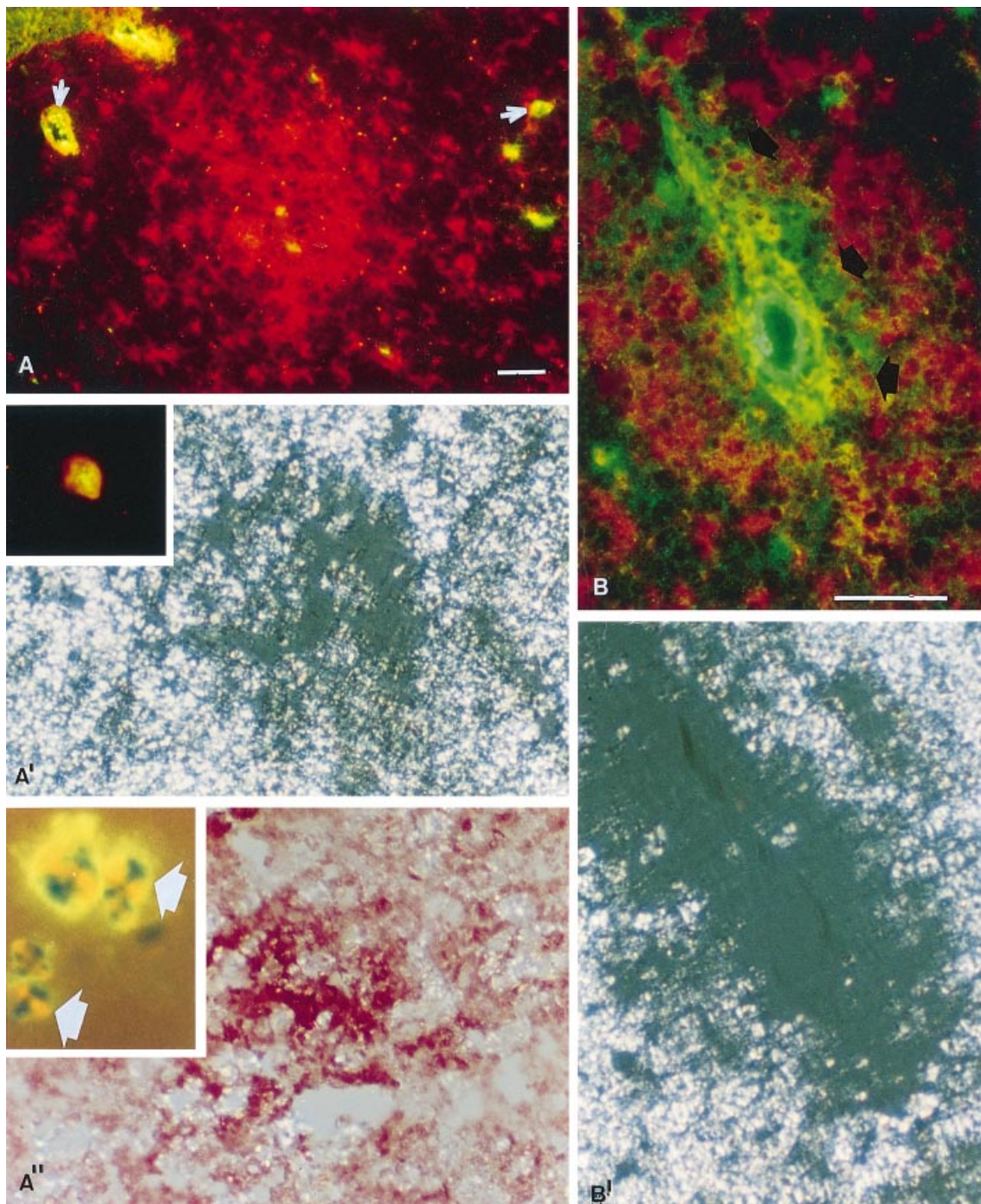


**Fig. 9** Immunocytochemistry of Type I lesions. (A) Focal Type I lesion located in the ventral spinocerebellar tract of the cord (Case B285). Frozen cross section, double labelled with fibrinogen-FITC and macrophage monoclonal EBM 11 and antimouse-TRITC, showing EBM<sup>+</sup> cells with microglial morphology, and fibrinogen reactivity restricted to the lumen of small vessels (arrows). (A') As in A, but observed with polarized light showing the focus of Grade 1+ demyelination. *Inset*: serial section, showing central vessel in A, double labelled for smooth muscle actin (HHF35-antimouse-TRITC) and fibrinogen-FITC. The arteriole is identified by positive reaction for smooth muscle and is positive for fibrinogen within the lumen. There is no evidence of leakage into the lesion parenchyma. (A'') Second serial section labelled for C3d showing complement reactions associated with microglial cells. Polyclonal rabbit anti-human C3d followed by biotinylated anti-rabbit and streptavidin-HRP-AEC, viewed with 50% polarized light. *Inset*: adjacent section to A''. Complement reactions (arrows) on the cytoplasmic membranes of microglial cells enclosing birefringent myelinic material is seen in detail by labelling with anti-human C3d-FITC and observing at high power with 50/50% blue/polarized light. Oil immersion. (B) Type I lesion showing development (transitional to Type II) with EBM 11<sup>+</sup> microglia (TRITC) and Grade 1+ fibrinogen leakage (FITC, arrows). (B') As in B, but viewed with polarized light, shows Grade 3+ demyelination in the lesion. Bars represent 50  $\mu$ m in A and B.

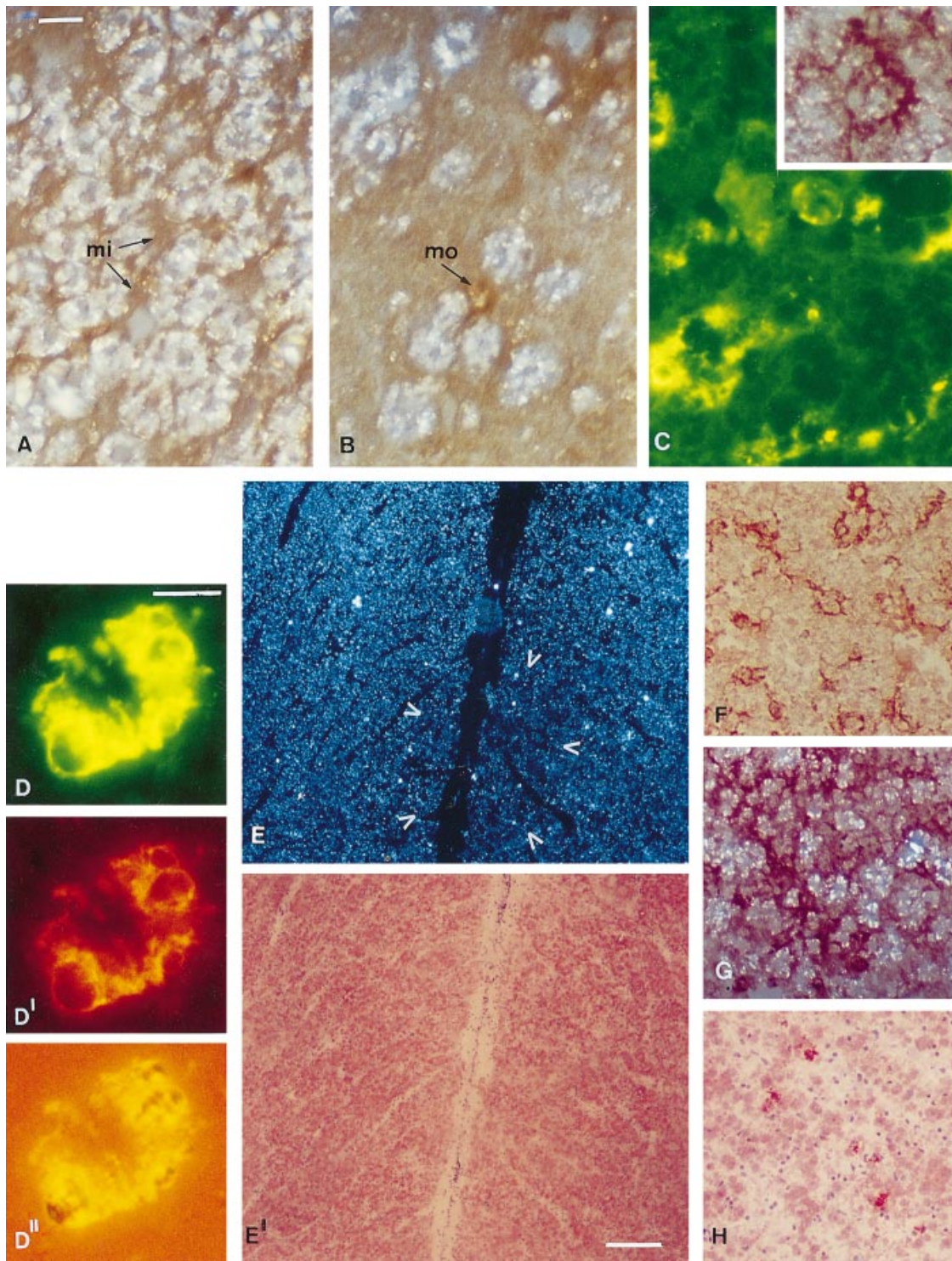


**Fig. 10** Immunocytochemistry of C3d/IgG<sup>+</sup> microglia. (A–C) Type I lesions with morphologically intact myelin sheaths in the long tracts of the cord. Class II positive microglia (mi), showing weak macrophage antibody reactivity (mo) are intercalated between morphologically intact myelinated axons. Polarized light (75%) with immunoperoxidase staining for HLA-DR, (A) and macrophage monoclonal EBM11 (B). (C) An adjacent section to A and B, reacted with rabbit anti-human C3d-FITC. Strong reactivity for complement is associated with microglia. *Inset*: microglia applied to the myelin sheath showing reactivity to the Membrane Attack Complex neo-antigen (C5–C9) (mouse monoclonal Ae.11 with biotinylated anti-mouse and streptavidin–HRP–AEC; polarized light). In A the bar represents 30  $\mu$ m. (D) Double labelled, periaxonal groups of microglia, pre-washed with acidic buffer, show strong, fixed, and colocalizing reactivity to C3d-FITC (D) and IgG-TRITC (D'), on the membranes of cytoplasmic vacuoles enclosing birefringent myelinic material. (D'') blue with 50% polarized light. In D the bar represents 5  $\mu$ m. (E–H) Polarized light detects a Grade 1+ area of minimal myelin abnormality in the anterior funiculus around the median fissure (arrows). The lesion is uniformly ORO negative (E'), but serial sections show class II (HLA-DR)<sup>+</sup> microglia (F), also positive for myelin basic protein neoantigen (clone 10) (G, with polarizer). Subsequent sections from this area (e.g. H) showed isolated pockets of cells with ORO<sup>+</sup> inclusions, Grade 1+. In E the bar represents 100  $\mu$ m.

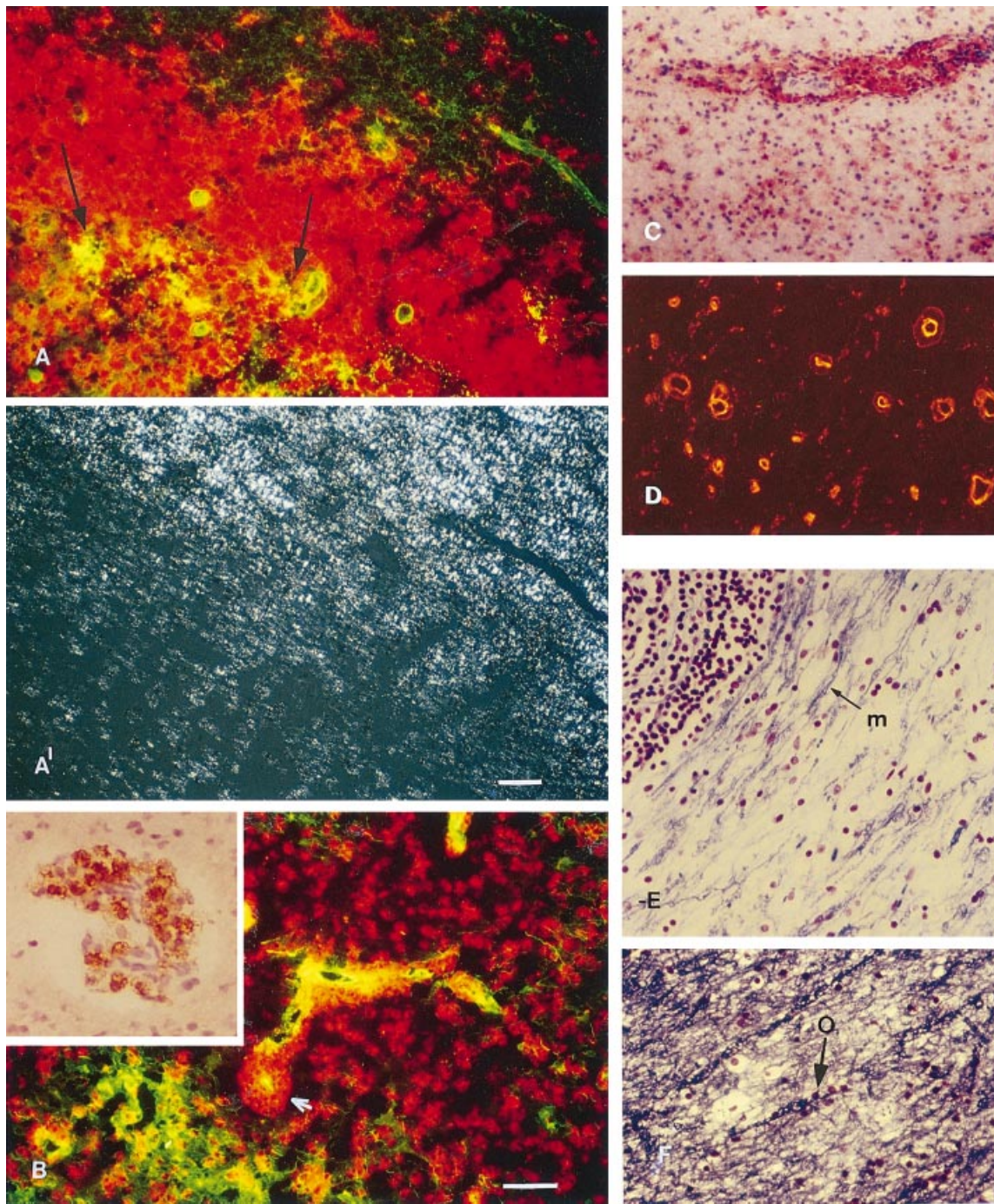
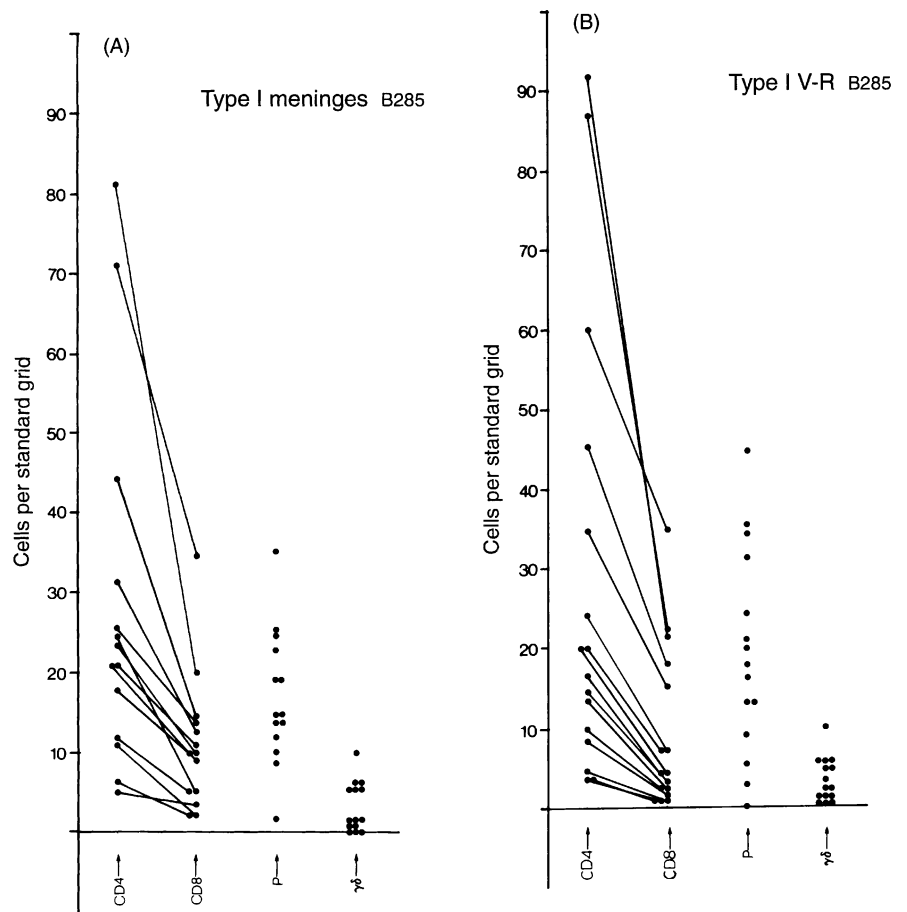


**Fig. 11** Histology and immunocytochemistry of lesion Types II and IV. (A) Type II plaque double labelled for macrophages (TRITC) and fibrinogen (FITC), viewed with combined TRITC-FITC blue/green fluorescence filters (A) and also with polarized light (A'). A typically high macrophage density is associated with Grade 3+ fibrinogen leakage (arrows) (Y1.82A with anti-mouse-TRITC and rabbit anti-human fibrinogen-FITC). The bar represents 50  $\mu$ m. (B) Double label for macrophages (TRITC) and human fibrinogen (FITC). The leaky centre of the lesion has a characteristically increased intensity of staining of perivascular macrophages (arrow), which are also reactive for the macrophage monoclonal RFD7 (*inset*) (EBM11 with anti-mouse-TRITC, and rabbit anti-human fibrinogen-FITC. RFD7 with anti-mouse-peroxidase-AEC). The bar represents 20  $\mu$ m. (C) Grade 4+ ORO inclusions in macrophages, showing a typical concentration of positive cells in the perivascular spaces. (D) Hypercellular central region of a Type II lesion labelled with CIV.22 anti-mouse-TRITC to detect Collagen IV. Grade 3+ collagen 'fragments'. (E and F) Type IV lesions. LFB staining showing chains of oligodendrocytes (o) and partial myelination (m). The lesions lack reactive astrocytes, have low (though LFB<sup>+</sup>) macrophage counts, and typically large accumulations of perivascular lymphocytes (E).



**Figs 12 A–K.** Inflammatory cell profiles for Type I and II multiple sclerosis lesions, multiple sclerosis spinal nerve roots and inflammatory controls. CD4<sup>+</sup>, CD8<sup>+</sup>,  $\gamma\delta$  and plasma (P) cell counts in tissue compartments, employing a standard grid at  $\times 20$ . Concurrent single field analysis of double-labelled CD4<sup>+</sup> and CD8<sup>+</sup> cells, with plasma and  $\gamma\delta$  cells in serial sections (*see Methods*). Men = meninges; VR = Virchow–Robin space; Par = parenchyma.

present it was most marked at the lesion edge. C3d/IgG complexes were not recorded in Type III lesions.

The Type IV data cluster represented a group of lesions with histological characteristics shared between Types I, II and III. These lesions were more or less equally represented with time (Fig. 8), and were characterized by the presence of oligodendroglia lying in close relation to partially myelinated sheaths (Fig. 11E and F). Type IV profiles found in cases 112.85 and B670 (Fig. 3), show that overall activity is low, total cell counts approach the normal range and giant reactive astrocytes are absent or rare. Collagen IV fragments were not seen but small numbers of LFB<sup>+</sup> macrophages were present, scattered throughout the lesions. Parenchymal fibrinogen (Grades 1 to 2+) was occasionally detected. Although inflammatory cell activity in the parenchyma of these lesions was low, they contained the largest perivascular accumulations of inflammatory cells recorded in this series (Fig. 11E). Unfortunately T-cell, ORO and C3d/IgG assessment was not possible due to lack of frozen tissues.

The small Type V data cluster (4.5% overall), was highly resolved in both types of analysis. The lesions represented were histologically ‘burnt out’ and inactive. Lesion profiles (*see* B9860, Fig. 2) show their close resemblance to the control chronic inactive lesions B9055 (Fig. 2) and B8946 (Fig. 3), 45 and 43 years duration, respectively. The Type V cluster lies in close proximity to Type I (Figs 4 and 5) on

account of the low cell counts but it is statistically differentiated by sub-normal cellularity.

### T-cell and plasma-cell profiles in Type I and II lesions

Type I and Type II lesions identified in frozen blocks from B285 (15 Type I, 10 Type II) and W69 (6 Type I, 12 Type II), were studied to quantify CD4<sup>+</sup>, CD8<sup>+</sup> and  $\gamma\delta$  T-cells and plasma cells within defined tissue compartments, using concurrent single field analysis as described in methods. Control tissues from C645 (perivenous encephalomyelitis), R62/86 (SSPE), and C1549 (glioma), were studied in parallel using identical methods. Cell profiles of classified lesions are shown in Fig. 12A–K, and the cell counts in these lesions and in the study overall are given in Table 4.

Multiple sclerosis and all the inflammatory controls showed a strong and remarkably stereotyped compartmentalization of the T-cell infiltrate. A marked predominance of CD4<sup>+</sup> over CD8<sup>+</sup> T-cells detected in the meninges, with CD4/CD8 ratios in the range 2.4–4.6, extended into the Virchow–Robin spaces in all cases (2.4–5.3). While there was a clear tendency for CD4<sup>+</sup> cells to remain within the perivascular spaces, the histological evidence indicated preferential CD8<sup>+</sup> cell migration across the glia limitans (Fig. 13A). This was

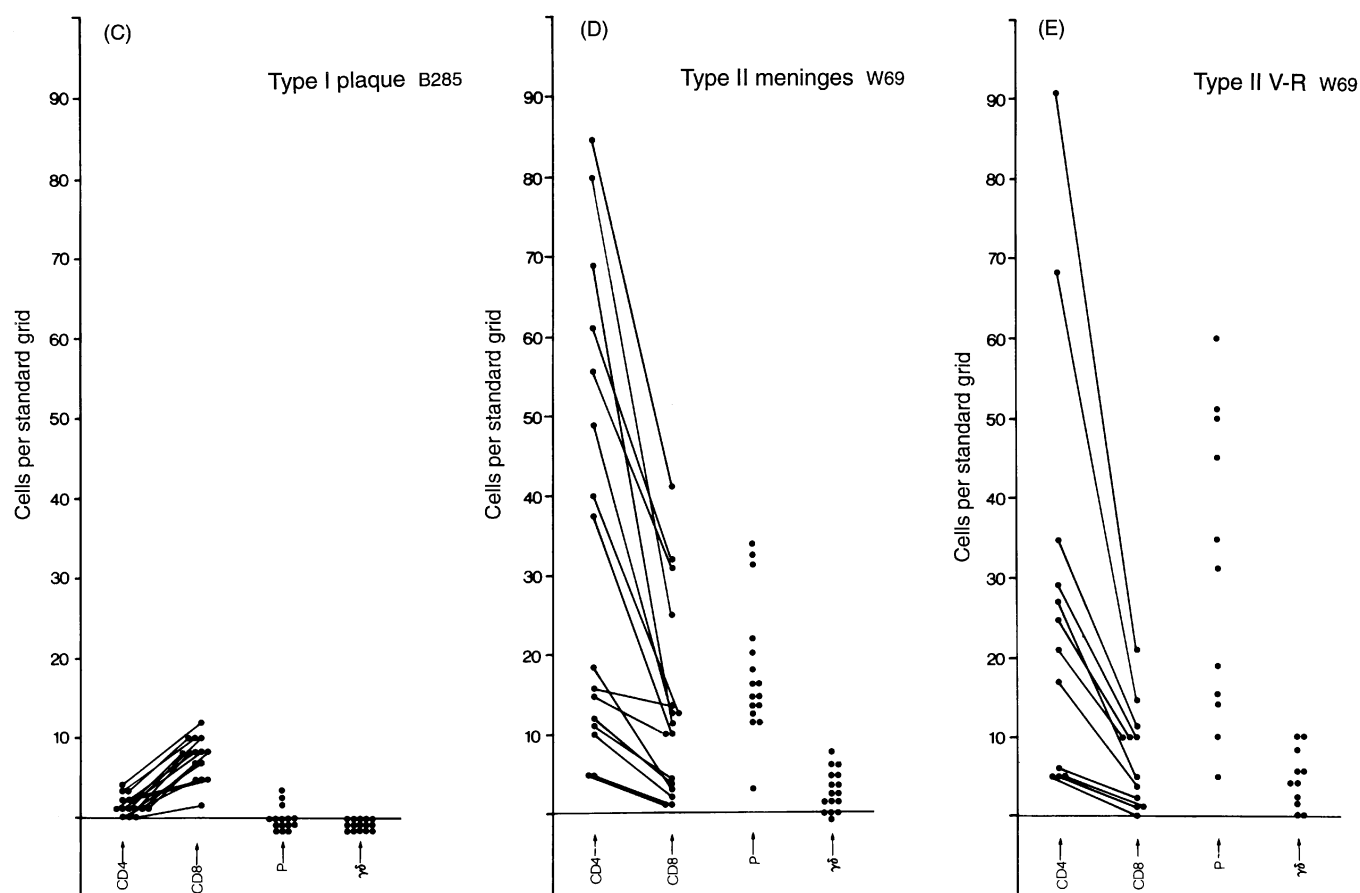


Fig. 12 continued

accompanied by a corresponding switch to CD8<sup>+</sup> dominance in the lesion parenchyma with CD4/CD8 ratios in the range 0.2–0.6. There was an overwhelming excess of parenchymal CD8<sup>+</sup> cells on the edge of the glioma (Fig. 12I) accompanied by CD4<sup>+</sup> dominance at the centre of the neoplasm. This tendency for parenchymal T-cells to be CD8<sup>+</sup> dominant at the lesion edge but CD4<sup>+</sup> dominant in the central parenchyma was a feature of the more complex, mature Type II multiple sclerosis plaques. Quantitative analysis using data contour plots of Type II lesions confirmed this feature (Fig. 14).

CD4<sup>+</sup> lymphocytes were initially undetected in the parenchyma of the 21 Type I lesions studied while the CD8<sup>+</sup> mean counts was recorded as  $7.0 \pm 2.4$  SEM per standard  $\times 20$  grid. However, by using immunostaining methods to increase CD4 detection (*see* Methods and Fig. 13B and B'), CD4<sup>+</sup> cells were found in the parenchyma of all but five of the 21 lesions studied, albeit in very small numbers ( $1.69 \pm 1.29$  SEM per  $\times 20$  standard grid).

A number of Type I lesions of particular interest were detected lying in close relation to the dorsal nerve root, in the region of the dorsal spinocerebellar and dorsolateral tracts and the substantia gelatinosa. This provided an opportunity to compare, in the same section, the inflammatory cell infiltrate of closely contiguous demyelinating CNS tissue

with normally myelinated nerve root. The CD4<sup>+</sup> cell count in the root parenchyma was  $1.54 \pm 1.41$  SEM, and in contiguous Type I lesions  $1.63 \pm 1.28$  SEM (not significant). However, the concurrent CD8<sup>+</sup> count was  $3.43 \pm 1.78$  SEM and  $7.54 \pm 2.76$  SEM, respectively ( $P < 0.0001$ ) (Table 4 and Fig. 12J and K).

Small numbers of  $\gamma\delta$  T-cells were detected in the parenchyma of Type II but not in Type I multiple sclerosis lesions.

Plasma cell counts in the parenchyma of Type I lesions were only slightly lower than CD4<sup>+</sup> T-cells, but within the Virchow–Robin spaces of these lesions and in adjacent meningeal tissues counts were high (Figs 12A and B, and 13C) and only slightly less than in SSPE. Type II parenchyma (Fig. 12F) contained plasma cells in numbers approaching, though significantly lower than, those of parenchymal CD4<sup>+</sup> T-cells ( $P < 0.001$ ). While the pattern of CD4<sup>+</sup> and CD8<sup>+</sup> cell distribution in perivenous encephalomyelitis (Fig. 12G) was qualitatively similar to multiple sclerosis and SSPE, T-cell numbers in all compartments, including the parenchyma, were greater in perivenous encephalomyelitis by a factor of 10. The overwhelming T-cell reactions in perivenous encephalomyelitis were observed in the virtual absence of plasma cells (Fig. 12G).

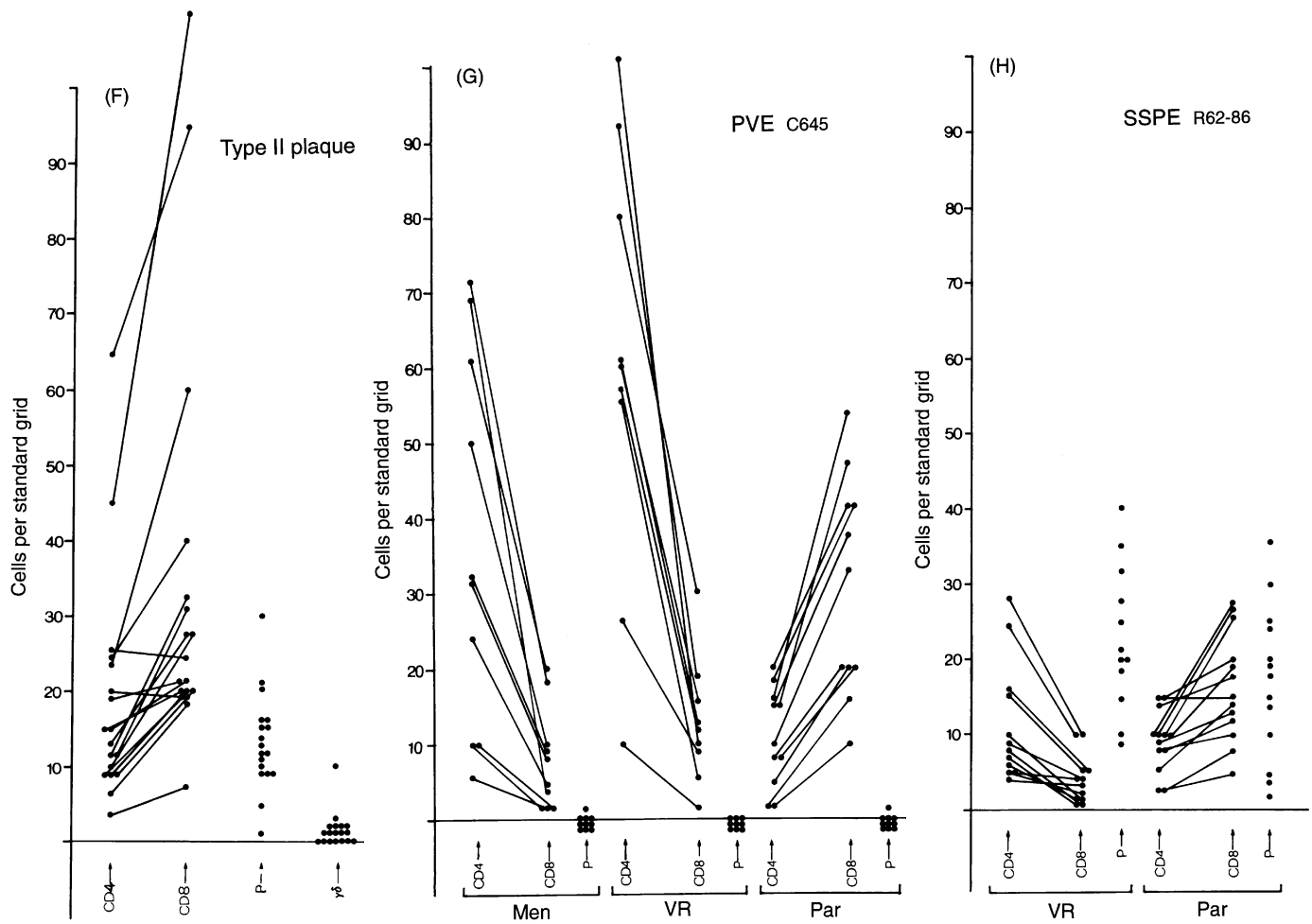


Fig. 12 continued

**Discussion**

We have shown that a statistical analysis of histological and immunocytochemical data may be used to categorize clinically early multiple sclerosis lesions into significantly distinct groups. Furthermore, the histological, statistical and clinical evidence supports the hypothesis that the groups identified represent key stages in early multiple sclerosis plaque morphogenesis, commencing with microglial activation in the parenchyma of both white and grey matter, and progressing to complex, focal hypercellular plaques in which myelin continues to be degraded within foamy macrophages, accompanied by giant astrocytosis. Progression, however, does not appear to be inevitable and may be interrupted by the development of lesions in which a much lower level of demyelination continues but is accompanied by oligodendroglial activity without astroglial activation.

A number of recent histological studies of multiple sclerosis autopsy tissues have attempted to provide a system of lesion grading to assist in identifying primary demyelinating plaques. Sanders *et al.* (1993), combining conventional histology with Class II MHC staining, descriptively grouped lesions from 52 cases (mean duration, 24.5 years) into four classes. Their Class I or 'pre-plaque' lesion, which they have

proposed as primary, consisted of an HLA-DR<sup>+</sup> but ORO-negative microglial nodule, in which demyelination was undetected. In a smaller series of 10 cases (mean duration 12 years), Li *et al.* (1993) used myelin degradation to separate 20 'active' plaques into four groups. Group I lesions, which they believe to be the earliest stage in demyelination, contained ORO<sup>+</sup> macrophages, also positive for myelin basic protein peptides, implying that cholesterol ester formation is an early event.

The autopsy tissues from our 13 cases with clinical histories ranging from 2 weeks to 10 years (mean 1.9 years), and with documented evidence of a terminal attack between 1 week and 10 months before death, represent a much earlier histological view of multiple sclerosis. With a more detailed histological analysis of multiple sclerosis lesions than has been reported to date, our results provide a quantitative basis for lesion grading which should help in the identification of key events in the pathogenesis of the disease.

We propose the Type I lesion as the primary demyelinating plaque in multiple sclerosis. These lesions significantly predominated in the earliest tissues but were rare after 5 weeks (Fig. 8). Unlike the microglial nodules described by Sanders *et al.* (1993) our Type I lesions show evidence of

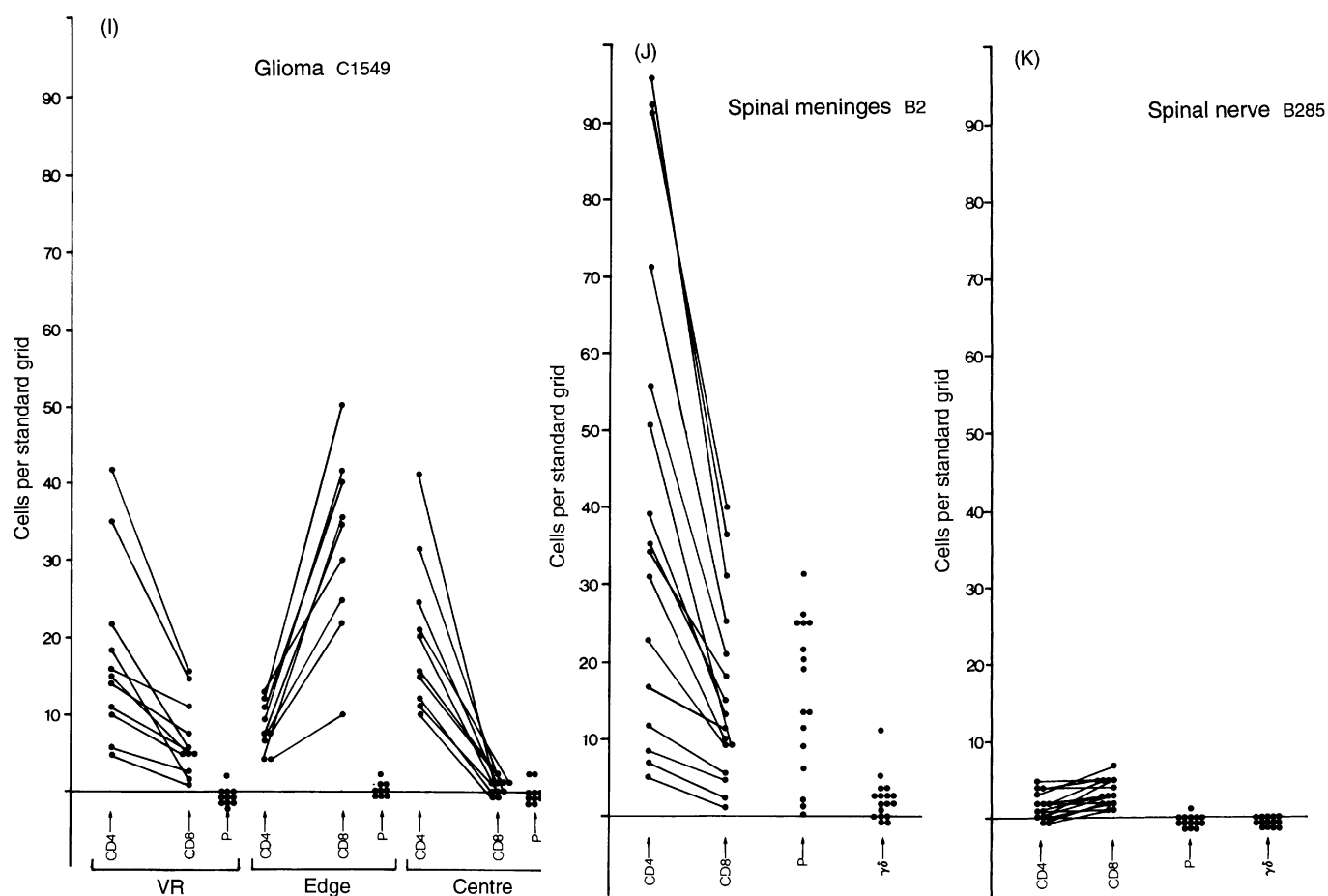


Fig. 12 continued

myelin phagocytosis and digestion. The absence of  $\text{ORO}^+$  inclusions in these zones contrasts with the Group I lesions of Li *et al.* (1993) and provides evidence that although myelin has been phagocytosed and intracytoplasmic myelin basic protein cleavage has commenced, lipid digestion with the production of cholesterol esters has not yet developed.

Type I lesions were found in both white and grey matter, either as groups of distinct microfoci or as more diffuse areas with 'geographical' margins. Lesions were situated around capillaries and venules, but also around arterioles, and immediately sub pial. The impression given by their location, morphology and immune reactivity, was of a diffusing, parenchymal, *in situ* activation of resident microglia, and this hypothesis is supported by the observation of close to normal total parenchymal cell counts. We cannot, however, be entirely confident that all of these cells come from the microglial pool. Remarkably, Type I lesions showed little or no histological evidence of fibrinogen leakage. While this does not necessarily indicate an intact blood-brain barrier, the appearance of subpial Type I lesions and lesions around muscular arteries, suggests that in these earliest stages the factor or factors inducing microglial activation, complement fixation and initial myelin phagocytosis, may gain access to the parenchyma across the pial membranes and the glia

limitans, from CSF and via Virchow-Robin spaces, before major disruption of the vascular endothelium is established.

The immune events within the parenchyma of Type I lesions, associated with the initiation of myelin phagocytosis were clearly humoral in emphasis. Deposits of IgG have been frequently described in unclassified multiple sclerosis lesions but they are readily washed away at neutral pH and are generally thought to represent non-specific and weak binding mediated by the Fc region of the IgG antibodies (Tavolato, 1975). To be significant in demyelination, immunoglobulins should be accompanied by other bound molecules including activated complement components. However, the observations of Prineas and Graham (1980) of the IgG capping of microglial cells applied to myelin sheaths has suggested that antibody-mediated demyelination may be important in the earliest stages of myelin phagocytosis.

However, surface IgG was also observed on microglia in ischaemic infarcts and in SSPE, raising doubts regarding its specificity in multiple sclerosis (Prineas, 1985). We have shown that microglial-bound, fixed complexes of IgG and complement, with evidence of complement activation, are a hallmark of the putative primary lesion in multiple sclerosis. These reactions were not found in our inflammatory control tissues including perivenous encephalomyelitis where early

**Table 4** Cell types in multiple sclerosis lesions

|   | CD4 <sup>+</sup> |               | CD8 <sup>+</sup> |               | CD4/CD8 |        | Plasma cells |               | γδ T cells |             |
|---|------------------|---------------|------------------|---------------|---------|--------|--------------|---------------|------------|-------------|
| Type I MS lesions (Cases B285 and W69, n = 21)    |                  |               |                  |               |         |        |              |               |            |             |
| Meninges  | 30.8 ± 24.0      | (28.5 ± 23.1) | 12.6 ± 10.2      | (11.2 ± 8.5)  | 2.44    | (2.54) | 20.7 ± 7.5   | (17.1 ± 8.6)  | 4.2 ± 3.6  | (3.6 ± 3.3) |
| VR space  | 30.7 ± 29.0      | (28.9 ± 28.4) | 12.6 ± 10.0      | (11.5 ± 10.4) | 2.44    | (2.51) | 18.7 ± 10.8  | (19.5 ± 13.1) | 4.0 ± 3.1  | (3.8 ± 2.5) |
| Parenchyma  | 1.7 ± 1.3        | (1.6 ± 1.3)   | 7.0 ± 2.4        | (7.5 ± 2.8)   | 0.24    | (0.22) | 1.0 ± 1.4    | (0.5)         | 0          | (0)         |
| Type II MS lesions (Cases B285 and W69, n = 22)   |                  |               |                  |               |         |        |              |               |            |             |
| Meninges  | 38.7 ± 26.0      | (35.6 ± 27.8) | 15.1 ± 14.6      | (13.6 ± 12.3) | 2.56    | (2.61) | 18.0 ± 9.5   | (17.9 ± 8.1)  | 3.7 ± 2.8  | (3.1 ± 2.4) |
| VR space  | 31.7 ± 28.0      | (28.2 ± 26.4) | 6.0 ± 5.8        | (7.8 ± 6.2)   | 5.28    | (3.64) | 31.3 ± 15.5  | (30.6 ± 18.8) | 4.8 ± 4.1  | (5.0 ± 3.5) |
| Parenchyma  | 21.1 ± 16.8      | (18.9 ± 15.1) | 35.8 ± 28.5      | (34.4 ± 27.6) | 0.59    | (0.55) | 15.2 ± 6.1   | (13.7 ± 6.5)  | 1.7 ± 2.5  | (1.4 ± 2.3) |
| Spinal nerve root (Case B285)                     |                  |               |                  |               |         |        |              |               |            |             |
| Meninges  | 45.8 ± 32.0      | (41.7 ± 31.3) | 17.1 ± 10.4      | (15.9 ± 11.8) | 2.68    | (2.62) | 17.8 ± 10.0  | (15.7 ± 9.7)  | 3.1 ± 2.9  | (2.5 ± 2.7) |
| Parenchyma  | 1.5 ± 1.4        | (1.7 ± 1.7)   | 3.5 ± 2.2        | (3.4 ± 1.8)   | 0.44    | (0.49) | 0.15         | (0.07)        | 0          | (0)         |
| Perivenous encephalomyelitis (Case C645)          |                  |               |                  |               |         |        |              |               |            |             |
| Meninges  | 36.5 ± 25.0      | (35.4 ± 26.0) | 8.0 ± 6.5        | (7.7 ± 6.1)   | 4.6     | (4.2)  | 0.2 ± 0.6    |               | Not done   |             |
| VR space  | 60.4 ± 29.1      | (58.6 ± 30.2) | 12.8 ± 8.0       | (12.1 ± 8.8)  | 4.7     | (4.8)  | 0            |               | Not done   |             |
| Parenchyma  | 10.9 ± 6.3       | (11.5 ± 7.0)  | 31.2 ± 14.6      | (30.5 ± 16.9) | 0.35    | (0.21) | 0.2 ± 0.6    |               | Not done   |             |
| Glioma (Case C1549)                               |                  |               |                  |               |         |        |              |               |            |             |
| VR space  | 17.6 ± 11.5      |               | 7.0 ± 5.0        |               | 2.5     |        | 0.2 ± 0.6    |               | Not done   |             |
| Edge  | 8.7 ± 2.9        |               | 32.2 ± 11.9      |               | 0.27    |        | 0.5 ± 1.0    |               | Not done   |             |
| Central   | 20.2 ± 9.9       |               | 0.6 ± 0.7        |               | 33.6    |        | 0.4 ± 0.8    |               | Not done   |             |
| Subacute sclerosing panencephalitis (Case R62.86) |                  |               |                  |               |         |        |              |               |            |             |
| VR space  | 11.5 ± 7.8       |               | 4.6 ± 3.1        |               | 2.5     |        | 22.7 ± 9.8   |               | Not done   |             |
| Parenchyma  | 9.2 ± 4.1        |               | 16.5 ± 7.4       |               | 0.56    |        | 17.0 ± 10.2  |               | Not done   |             |

CD4<sup>+</sup>, CD8<sup>+</sup>, γδ T cells and plasma cell counts in tissue compartments of type I and type II multiple sclerosis lesions, spinal nerve root and inflammatory controls (Cases C645, R62.86 and C1549). Overall mean values (per standard ×20 grid, using not <20 grids) ± SD (values in brackets for the cell profiles of Fig. 12). VR space = Virchow–Robin space.

primary demyelination is a cardinal feature. The disappearance of these reactions as multiple sclerosis plaques mature suggests that the inflammatory mechanisms initiating demyelination in the multiple sclerosis lesion may be quite different from the mechanisms operating in maturing and established plaques. A recent report of a diffusing factor in Balo's concentric sclerosis, which was inhibited using immunoadsorption plasmapheresis (Sekijima *et al.*, 1997), has provided further evidence for the role of antibody in initial demyelination.

Parenchymal CD4<sup>+</sup> T-cells were not detected in a proportion of Type I lesions and, when present, they were seen in very small numbers and invariably accompanied by a larger CD8<sup>+</sup> infiltrate. However, parenchymal CD4<sup>+</sup> infiltration increased concomitant with plaque maturation so that in Type II lesions the relative dispositions of CD4<sup>+</sup> and CD8<sup>+</sup> T-cells carried the hallmark of a balance of opposing (helper versus suppressor) forces, as is seen in various chronic inflammatory and neoplastic lesions (*see* Fig. 14). The rarity of γδ T-cells in Type I lesions and their weak association with Type II lesions suggests a secondary role for these cells in lesion maturation.

Positive reactions for the C9 neoantigen within the myelin sheath–macrophage membrane interface, implies complement activation and the formation of the membrane attack complex (C5–C9). This requires the transient production of C5–7 which is capable, in free solution, of binding to any lipid bilayer to produce 'reactive lysis' on bystander cells. The myelin sheath is unlikely to escape damage in these reactions,

and the phagocytic activity of the activated microglia may be mediated, at least in part, by scavenger receptors capable of recognizing denatured tissue components.

In contrast to the findings of Hays *et al.* (1988) in the antibody-mediated demyelinating peripheral neuropathies, we were unable to detect any complement or immunoglobulin on the myelin sheath itself or on myelinic debris. This does not support the attractive hypothesis that the myelin sheath is the primary target of humoral immune reactions, or that antibody-mediated opsonization may account for demyelination in primary lesions. However, the presence of C3d/IgG complexes bound to microglial membranes can be expected to be potent in inducing cellular activation. While microglial activation may be induced in Type I lesions by diffusing cytokines, CNS macrophages are known to be activated by a wide variety of inflammatory and non-inflammatory stimuli, none of which produce demyelinating plaques. This points to the involvement of a rather more specific or more potent immune activation, and an alternative explanation is that pathogenic antigens contained within immune complexes (Coyle, 1987), and initially processed within the Virchow–Robin spaces, may spread into the parenchyma across the glia limitans.

If such putative antigens are derived from CNS tissue, we are not able to account for the lack of localization of fixed C3d and immunoglobulin on the myelin sheath or on other parenchymal tissues. On the other hand if the antigens are extrinsic, and by implication, microbial, they may gain access to the lesion parenchyma across the glia limitans

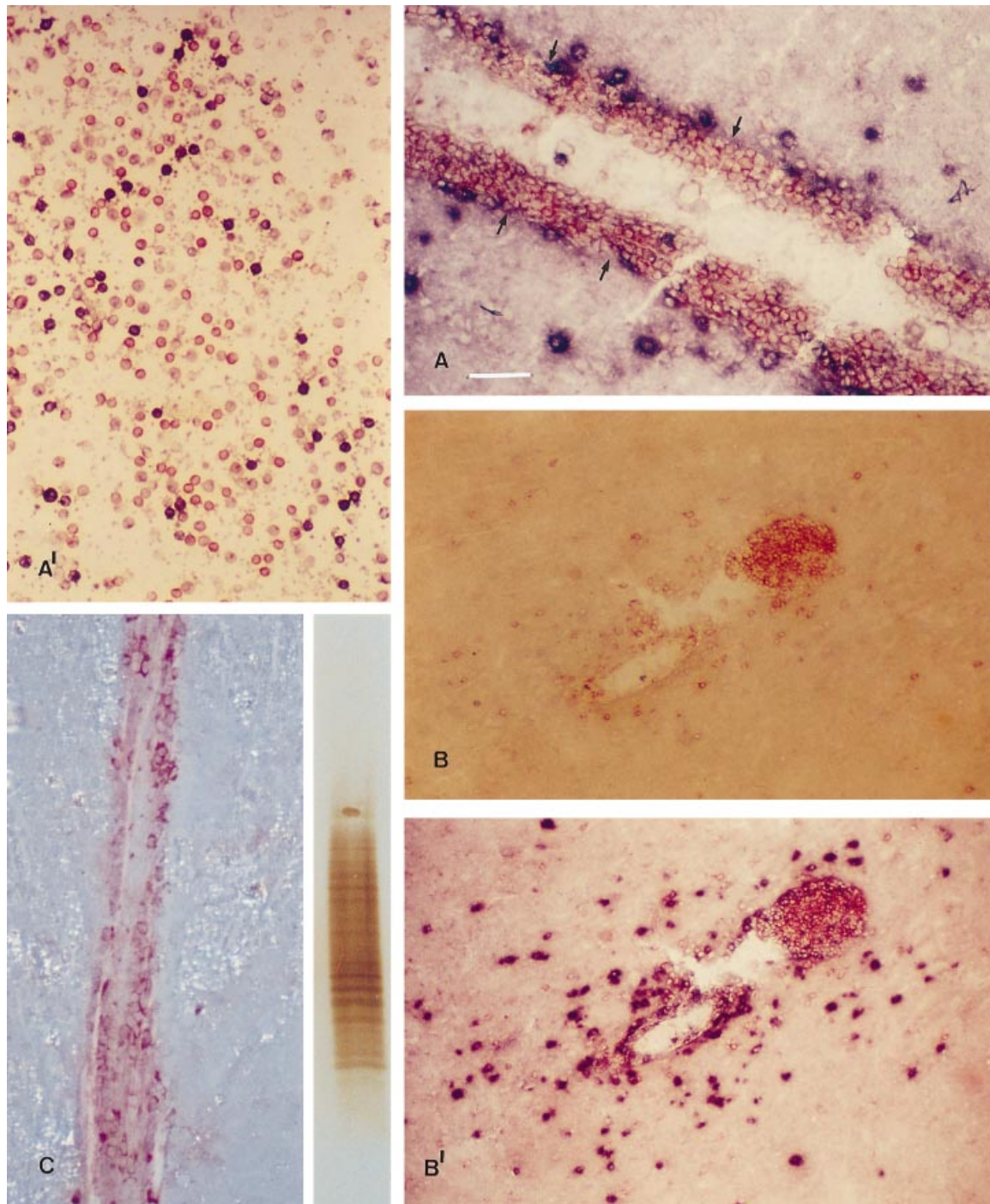


**Fig. 13** Concurrent single field analysis of lymphocytes. (A) Double labelling for CD4<sup>+</sup> and CD8<sup>+</sup> T lymphocytes. Cryostat section of a venule in an advanced Type I multiple sclerosis lesion, double labelled for CD4 (brown-red) and CD8 (blue-purple) T-cells. Biotinylated anti-CD4, MT.310 (IgG) with streptavidin-HRP-AEC, and anti-CD8, RFT8 (IgM) with anti-mouse IgM, phosphatase-NBT. Brown/red cells (CD4<sup>+</sup>), are concentrated typically in the perivascular space, while the blue/purple cells (CD8<sup>+</sup>) are distributed along the glia limitans (arrows) and in the perivascular parenchyma. The bar represents 20  $\mu$ m. (A') Reagent/observer control. Ficoll purified peripheral blood leucocytes double labelled in parallel for CD4<sup>+</sup> and CD8<sup>+</sup> T cells. CD4<sup>+</sup>/CD8<sup>+</sup> ratio =  $2.15 \pm 0.11$  SEM. (B) Technique to increase sensitivity in CD4<sup>+</sup> T-cell detection. After labelling for both CD4 and CD8 T-cells (*see Methods*), preliminary CD4<sup>+</sup> (AEC) development and counting in a wet preparation (B) was followed by development (B') of NBT, to detect CD8<sup>+</sup> cells. (C) Adjacent section of vessel in A, labelled with rabbit anti-human immunoglobulins IgG, IgA and IgM (F(ab')<sub>2</sub>) with anti-rabbit HRP-AEC. The perivascular space contains numerous immature immunoglobulin-containing plasma cells. Polarized light (50%) shows Grade 1+ perivascular demyelination. *Inset*: aqueous extract of adjacent tissue section contains cathodic oligoclonal bands of IgG (Agarose IEF of 5  $\mu$ l extract; method of Walker *et al.*, 1983.)

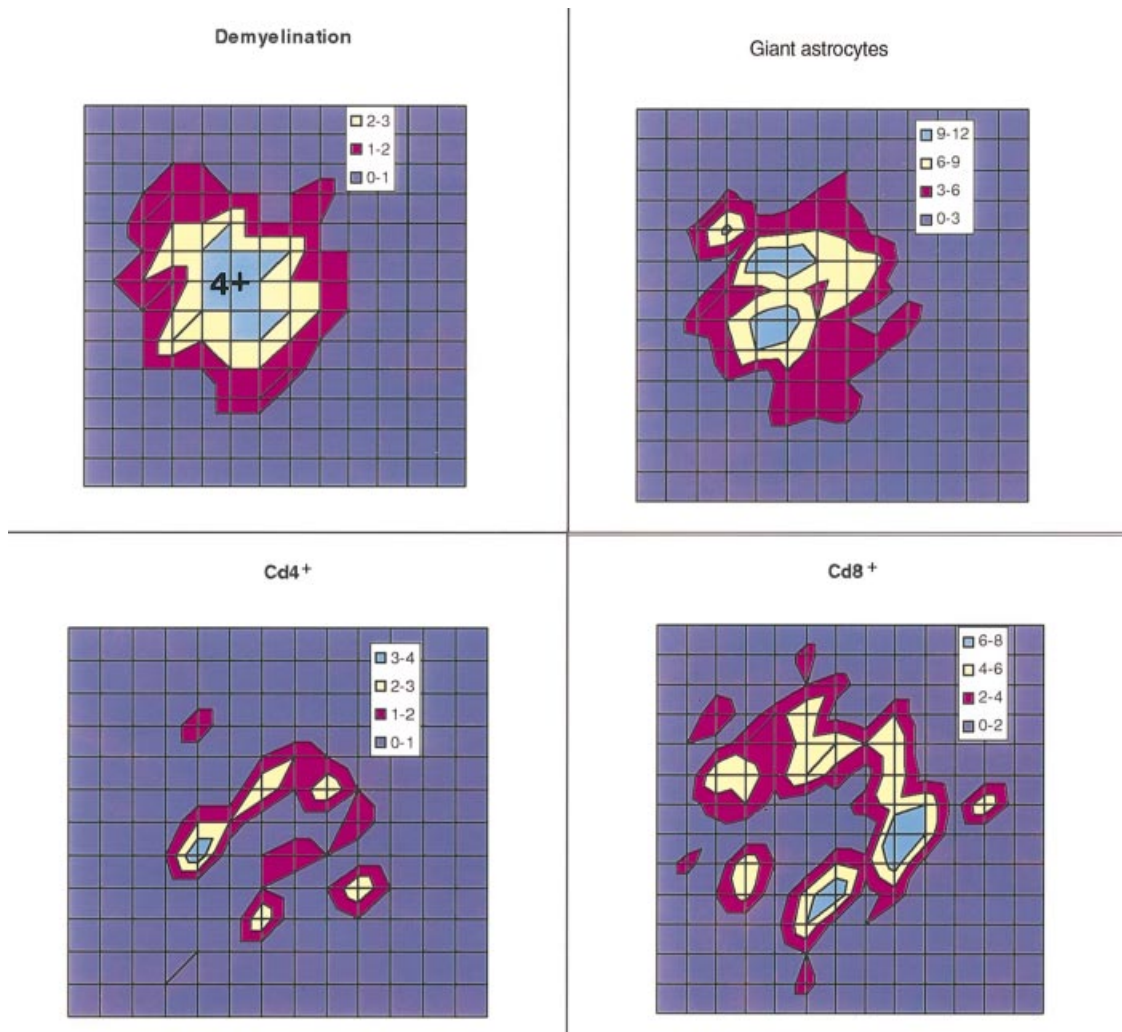


**Fig. 14** Data contour plot of a typical Type II lesion, double labelled for CD4<sup>+</sup> and CD8<sup>+</sup> T-cells. Demyelination (Grades 0 to 4+) was recorded using polarized light (*top left*) to locate the lesion. Giant (reactive) astrocytes were counted per standard grid, and concurrently with parenchymal CD4<sup>+</sup> and CD8<sup>+</sup> cells. The lesion is characterized by central demyelination and gliosis, with an inner ring of CD4<sup>+</sup> Tcells and an outer ring of CD8<sup>+</sup> T cells at the plaque edge.

having gained the perivascular compartment via CSF, as was originally postulated by Dawson (1916).

The presence of numerous plasma cells around and within Type I lesions is indicative of a strong B-cell response at this early stage and at the site of primary lesion development. A comparison of the T-cell response at 14 days since clinical onset in perivenous encephalomyelitis (C 645) and at 7 days with acute multiple sclerosis (B 285) is shown in Fig. 12C and G. This data shows that the early demyelinating immune response in perivenous encephalomyelitis is, in sharp contrast to multiple sclerosis, overwhelmingly T cell in emphasis.

It is remarkable that the level of CD4<sup>+</sup> T-cell activity measured in normally myelinated nerve root does not differ significantly from contiguous demyelinating Type I lesions in central white matter. In contrast, however, parenchymal CD8<sup>+</sup> cells were significantly raised in these lesions (Fig. 12C). This observation is difficult to interpret as the preferential migration of CD8<sup>+</sup> cells across the glia limitans

is seen in all our inflammatory controls and we have not been able to detect Class I antigens in Type I lesions on any structures other than vascular endothelial cells and on the perivascular and parenchymal lymphocytes themselves (our unpublished data).

In view of the evidence of very different immune processes at different stages of early plaque morphogenesis, future immunohistological studies to investigate the pathogenesis of plaques will need to define the staging of the lesions being studied clearly.

This study points strongly to a key role for activated microglia in initial demyelination in multiple sclerosis, and supports Prineas' contention (1985) that the 'war zone' in this disease is primarily at the macrophage–myelin interface. If this is so, therapeutic strategies to inhibit macrophage activity such as proteinase inhibitors, may be of greater benefit than efforts to inhibit T cells or other immune reactions.

A second implication of these observations is that further analysis of the oligoclonal B-cell response in the early stages of multiple sclerosis, and especially the IgM response (Sharief and Thompson, 1991), may be productive in the search for antibody directed against key pathogenic antigens, be they CNS or microbial in origin.

### Acknowledgements

We are indebted to the late Professor C. W. M. Adams who provided Cases 112.85, P72.479, 183.86, 248.83 and P63.324, and much helpful advice and encouragement. We wish to thank Dr M. L. Rossie who supplied Case W69, also Dr J. Newcombe for Case B285, Dr R. Poston for Cases B303 and B260.Q7, Professor G. Janossy for monoclonal antibodies RFD 7 and RFT 8, Dr N. Groome for Clone 10, and Dr J. Newcombe for 14 E. The work was supported in part by grants from the Multiple Sclerosis Society of Great Britain and Northern Ireland, Action for Research into Multiple Sclerosis, The Disabilities Study Unit and the Medical Research Council.

### References

- Adams CWM. Pathology of multiple sclerosis: progression of the lesion. [Review]. *Br Med Bull* 1977; 33: 15–20.
- Adams CWM. Vascular aspects of multiple sclerosis. In: Adams CWM. A colour atlas of multiple sclerosis and other myelin disorders. London: Wolfe Medical, 1989: 184–7.
- Adams CWM, Poston RN, Buk SJ. Pathology, histochemistry and immunocytochemistry of lesions in acute multiple sclerosis. *J Neurol Sci* 1989; 92: 291–306.
- Banfield JD, Raftery AE. Model based Gaussian and non-Gaussian clustering. *Biometrics* 1993; 49: 803–22.
- Brosnan CF, Cannella B, Battistini L, Raine CS. Cytokine localization in multiple sclerosis lesions: correlation with adhesion molecule expression and reactive nitrogen species. [Review]. *Neurology* 1995; 45 (6 Suppl 6): S16–21.
- Compston DAS, Morgan BP, Campbell AK, Wilkins P, Cole G, Thomas ND, et al. Immunocytochemical localization of the terminal complement complex in multiple sclerosis. *Neuropathol Appl Neurobiol* 1989; 15: 307–16.
- Coyle P. Analysis of immune complexes in multiple sclerosis. In: Lowenthal A, Raus J, editors. Cellular and humoral immunological components of cerebrospinal fluid in multiple sclerosis. New York: Plenum Press, 1987: 129–37.
- Davey FR, Cordell JL, Erber WN, Pulford KAF, Gatter KC, Mason DY. Monoclonal antibody (Y1/82A) with specificity towards peripheral blood monocytes and tissue macrophages. *J Clin Pathol* 1988; 41: 753–8.
- Dawson JW. The histology of disseminated sclerosis. *Trans Roy Soc Edin* 1916; 50: 517–740.
- Esiri MM. Immunoglobulin-containing cells in multiple sclerosis plaques. *Lancet* 1977; 2: 478.
- Esiri MM. Multiple sclerosis: a quantitative and qualitative study of immunoglobulin-containing cells in the central nervous system. *Neuropathol Appl Neurobiol* 1980; 6: 9–21.
- Esiri MM, Gay D. Immunological and neuropathological significance of the Virchow-Robin space. [Review]. *J Neurol Sci* 1990; 100: 3–8.
- Esiri MM, Gay D. The immunocytochemistry of multiple sclerosis plaques. In: Raine CS, McFarland HF, Tourtellotte WW, editors. Multiple sclerosis. Clinical and pathogenetic basis. London: Chapman and Hall, 1997: 173–85.
- Esiri MM, Reading MC. Macrophage populations associated with multiple sclerosis plaques. *Neuropathol Appl Neurobiol* 1987; 13: 451–65.
- Esiri MM, Oppenheimer DR, Brownell B, Haire M. Distribution of measles antigen and immunoglobulin-containing cells in the CNS in subacute sclerosing panencephalitis (SSPE) and atypical measles encephalitis. *J Neurol Sci* 1982; 53: 29–43.
- Esiri MM, Reading MC, Squier MV, Hughes JT. Immunocytochemical characterization of the macrophage and lymphocyte infiltrate in the brain in six cases of human encephalitis of varied aetiology. *Neuropathol Appl Neurobiol* 1989; 15: 289–305.
- Everitt BS. Cluster analysis. 3rd ed. London: Edward Arnold, 1993.
- Fabry Z, Raine CS, Hart MN. Nervous tissue as an immune compartment: the dialect of the immune response in the CNS. [Review]. *Immunol Today* 1994; 15: 218–24.
- Fowlkes EB, Mallows CL. A method for comparing two hierarchical clusterings. *J Am Stat Assoc* 1983; 78: 553–69.
- Franklin WA, Mason DY, Pulford K, Falini B, Bliss E, Gatter KC, et al. Immunohistological analysis of human mononuclear phagocytes and dendritic cells by using monoclonal antibodies. *Lab Invest* 1986; 54: 322–35.
- Gay D, Esiri M. Blood-brain barrier damage in acute multiple sclerosis plaques. An immunocytological study. *Brain* 1991; 114: 557–72.
- Groome N, Harland J, Dawkes A. Preparation and properties of monoclonal antibodies to myelin basic protein and its peptides. *Neurochem Int* 1985; 7: 309–17.
- Hafler DA, Weiner HL. MS: a CNS and systemic autoimmune disease. [Review]. *Immunol Today* 1989; 10: 104–7.
- Hays AP, Lee SSL, Latov N. Immune reactive C3d on the surface of myelin sheaths in neuropathy. *J Neuroimmunol* 1988; 18: 231–44.
- Janossy G, Bofill M, Poulter LW, Rawlings E, Burford GD, Navarrete C, et al. Separate ontogeny of two macrophage-like accessory cell populations in the human fetus. *J Immunol* 1986; 136: 4354–61.
- Li H, Newcombe J, Groome NP, Cuzner ML. Characterization and distribution of phagocytic macrophages in multiple sclerosis plaques. *Neuropathol Appl Neurobiol* 1993; 19: 214–23.
- Linnington C, Lassmann H, Morgan BP, Compston DAS. Immunohistochemical localisation of terminal complement component C9 in experimental allergic encephalomyelitis. *Acta Neuropathol (Berl)* 1989; 79: 78–85.
- Lucchinetti CF, Bruck W, Rodriguez M, Lassmann H. Distinct

- patterns of multiple sclerosis pathology indicates heterogeneity on pathogenesis. [Review]. *Brain Pathol* 1996; 6: 259–74.
- McCallum K, Esiri MM, Tourtellotte WW, Booss J. T cell subsets in multiple sclerosis. Gradients at plaque borders and differences in nonplaque regions. *Brain* 1987; 110: 1297–308.
- Newcombe J, Cuzner ML. Monoclonal antibody 14E identifies the oligodendrocyte cell body in normal adult human and rat white matter. *J Neuroimmunol* 1988; 19: 11–20.
- Pambakian S, Poston RN. The binding of immunoglobulin Fc to cationic proteins. *Clin Exp Immunol* 1987; 68: 402–8.
- Pelfrey CM, Tranquill LR, Vogt AB, McFarland HF. T cell response to two immunodominant proteolipid protein (PLP) peptides in multiple sclerosis patients and healthy controls. *Multiple Sclerosis* 1996; 1: 270–8.
- Prineas JW. Multiple sclerosis: presence of lymphatic capillaries and lymphoid tissue in the brain and spinal cord. *Science* 1979; 203: 1123–5.
- Prineas JW. The neuropathology of multiple sclerosis. In: Vinken PJ, Bruyn GW, Klawans HL, editors. *Handbook of clinical neurology*, Vol. 47. Amsterdam: Elsevier, 1985: 213–57.
- Prineas JW, Graham JS. Multiple sclerosis: capping of surface immunoglobulin G on macrophages engaged in myelin breakdown. *Ann Neurol* 1980; 10: 149–58.
- Raine CS. Multiple sclerosis: immune system molecule expression in the central nervous system. [Review]. *J Neuropathol Exp Neurol* 1994; 53: 328–37.
- Rand WM. Objective criteria for the evaluation of clustering methods. *J Amer Stat Assoc* 1971; 66: 846–50.
- Ransohoff RM, Tuohy V, Lehmann P. The immunology of multiple sclerosis: new intricacies and new insights. [Review]. *Curr Opin Neurol* 1994; 7: 242–9.
- Rennels ML, Gregory TF, Blaumanis OR, Fujimoto K, Grady PA. Evidence for a 'paravascular' fluid circulation in the mammalian central nervous system, provided by the rapid distribution of tracer protein throughout the brain from the subarachnoid space. *Brain Res* 1985; 326: 47–63.
- Sanders V, Conrad AJ, Tourtellotte WW. On classification of post-mortem multiple sclerosis plaques for neuroscientists. *J Neuroimmunol* 1993; 46: 207–16.
- Sekijima Y, Tokuda T, Hashimoto T, Koh C-S, Shoji S, Yanagisawa N. Serial magnetic resonance imaging (MRI) study of a patient with Balo's concentric sclerosis treated with immunoadsorption plasmapheresis. *Multiple Sclerosis* 1997; 2: 291–4.
- Sharief MK, Thompson EJ. Intrathecal immunoglobulin M synthesis in multiple sclerosis. *Brain* 1991; 114: 181–95.
- Tavolato BF. Immunoglobulin G distribution in multiple sclerosis brain. An immunofluorescence study. *J Neurol Sci* 1975; 24: 1–11.
- Tsakada T, McNutt MA, Ross R, Gown AM. HHF35, a muscle actin-specific monoclonal antibody: II. Reactivity in normal, reactive, and neoplastic human tissues. *Am J Pathol* 1987; 127: 389–402.
- Utz U, McFarland HF. The role of T cells in multiple sclerosis: implications for therapies targeting the T cell receptor. [Review]. *J Neuropathol Exp Neurol* 1994; 53: 351–8.
- Venables WN, Ripley BD. *Modern applied statistics with S-PLUS*. New York: Springer-Verlag, 1994.
- Walker RWH, Keir G, Johnson MH, Thompson EJ. A rapid method for detecting oligoclonal IgG in unconcentrated CSF, by agarose isoelectric focusing, transfer to cellulose nitrate and immunoperoxidase staining. *J Neuroimmunol* 1983; 4: 141–8.
- Woodroffe MN. Cytokine production in the central nervous system. [Review]. *Neurology* 1995; 45(6 Suppl 6): S6–10.
- Zhang ET, Richards HK, Kida S, Weller RO. Directional and compartmentalised drainage of interstitial fluid and cerebrospinal fluid from the rat brain. *Acta Neuropathol (Berl)* 1992; 83: 233–9.

*Received February 25, 1997. Accepted March 20, 1997*

## Appendix 1 Autopsy cases

| Case | Autopsy number | Age (years) | Sex | Clinical diagnosis  | Total duration | Duration of terminal illness | Histological diagnosis       | Lesions studied (n) | Previously published data in each case |
|------|----------------|-------------|-----|---------------------|----------------|------------------------------|------------------------------|---------------------|--|
| 1    | B670*          | 32          | M   | Acute MS            | 2 years        | 10 months                    | 'Severe MS'                  | 27                  | Nil                                    |
| 2    | 112/85         | 60          | M   | Acute MS            | 26 weeks       | 26 weeks                     | Acute MS                     | 10                  | Adams <i>et al.</i> (1990) (19)        |
| 3    | P72/479*       | 45          | M   | Acute MS            | 2 weeks        | 2 weeks                      | Acute brainstem MS           | 12                  | Adams <i>et al.</i> (1990) (5)         |
| 4    | W69            | 26          | F   | Acute MS            | 4 months       | 2 months                     | Fulminating MS               | 20                  | Esiri and Reading (1987) (1)           |
| 5    | B9860          | 52          | F   | Acute MS            | 2 years        | 1 month                      | Acute MS                     | 10                  | Esiri and Reading (1987) (2)           |
| 6    | B561           | 51          | F   | Acute MS            | 2 years        | 1 week                       | Acute MS                     | 8                   | Esiri (1977)                           |
| 7    | 1413           | 26          | F   | Acute MS            | 15 months      | 2 months                     | Acute MS                     | 6                   | Nil                                    |
| 8    | B285           | 35          | M   | Acute MS            | 6 months       | 1 week                       | Acute MS                     | 31                  | Gay and Esiri (1991) (5)               |
| 9    | B260Q7         | 33          | F   | Progressive MS      | 10 years       | 6 months                     | Chronic active MS            | 4                   | Gay and Esiri (1991) (4)               |
| 10   | B303           | 43          | F   | Acute MS            | 2 years        | 6 months                     | Acute MS                     | 6                   | Gay and Esiri (1991) (6)               |
| 11   | 183/86         | 23          | F   | Brainstem MS        | 5 weeks        | 5 weeks                      | Acute MS                     | 5                   | Adams <i>et al.</i> (1990) (10)        |
| 12   | 248/83         | 52          | F   | Acute pontine MS    | 4 years        | 12 weeks                     | Acute MS                     | 8                   | Adams <i>et al.</i> (1990) (16)        |
| 13   | P63/324*       | 44          | F   | Brainstem MS        | 20 weeks       | 20 weeks                     | Acute MS                     | 8                   | Adams <i>et al.</i> (1990) (18)        |
| 14   | B9055          | 65          | F   | Chronic inactive MS | 45 years       | 2 months                     | Chronic inactive MS          | 2                   | Esiri and Reading (1987) (8)           |
| 15   | B8946          | 61          | F   | Chronic inactive MS | 43 years       | 6 months                     | Chronic inactive MS          | 2                   | Esiri and Reading (1987) (7)           |
| 16   | C645           | 20          | M   | Acute encephalitis  | 2 weeks        | 2 weeks                      | Perivenous encephalomyelitis | 4 blocks            | Esiri <i>et al.</i> (1989)             |
| 17   | 458/87         | 18          | F   | SSPE                | 13 years       |                              | Measles SSPE                 | 4 blocks            | Esiri <i>et al.</i> (1989)             |
| 18   | R62/86         | 15          | M   | SSPE                | 12 months      |                              | Measles SSPE                 | 2 blocks            | Esiri <i>et al.</i> (1982)             |
| 19   | C1229          | 15          | F   | RTA                 |                | 30 min                       | Traumatic haemorrhage        |                     |  |
| 20   | C1225          | 38          | M   | RTA                 |                | 30 h                         | Contracoup contusion         |                     |  |
| 21   | C1248          | 18          | F   | RTA                 |                | 36 h                         | Sub dural haematoma          |                     |  |
| 22   | C1231          | 19          | M   | RTA                 |                | 24 h                         | Sub dural haematoma          |                     |  |
| 23   | C1087          | 15          | F   | Epilepsy            |                |                              | R Hemispherectomy            |                     |  |
| 24   | C1226          | 54          | M   | Pancreas carcinoma  |                |                              | Sagittal sinus thrombosis    |                     |  |
| 25   | C1549          |             |     | Cerebral neoplasm   |                |                              | Glioma                       |                     |  |
| 26   | C1557          |             |     | Cerebral neoplasm   |                |                              | Glioma                       |                     |  |

MS = multiple sclerosis; SSPE = subacute sclerosing panencephalitis; RTA = road traffic accident. \*Paraffin sections only.

## Appendix 2 Monoclonal and polyclonal antibodies employed

| Antibody to:            | Antigen source | Antibody source            | Labels employed | Second antibody                 | Source of primary antibody    |
|-------------------------|----------------|----------------------------|-----------------|---------------------------------|-------------------------------|
| Collagen IV             | Human          | Mouse mc CIV 22            | na              | Rabbit-anti-mouse TRITC         | Bionuclear, Dako              |
| Laminin                 | Human          | Mouse mc                   | na              | Rabbit-anti-mouse FITC          | Serotec                       |
| Actin                   | Human          | Mouse mc HHF 35            | na              | Rabbit-anti-mouse TRITC         | Tsukada <i>et al.</i> (1987)  |
| Actin                   | Human          | Mouse mc 1A4               | na              | Rabbit-anti-mouse peroxidase    | Dako                          |
| Fibrinogen              | Human          | Rabbit                     | FITC            | na                              | Dako                          |
| Complement C3d          | Human          | Rabbit                     | FITC            | na                              | Dako                          |
| Complement C5b-9        | Human          | Mouse mc aE11              | na              | Rabbit-anti-mouse peroxidase    | Dako                          |
| Macrophage              | Human          | Mouse mc Y1/82A            | na              | Rabbit-anti-mouse TRITC         | Davey <i>et al.</i> (1988)    |
| Macrophage              | Human          | Mouse mc EBM 11            | na              | Rabbit-anti-mouse FITC          | Franklin <i>et al.</i> (1986) |
| Macrophage              | Human          | Mouse mc RFD 7             | na              | Rabbit-anti-mouse peroxidase    | Janosy <i>et al.</i> (1986)   |
| Macrophage              | Human          | Mouse mc HAM 56            | na              | Rabbit-anti-mouse peroxidase    | Dako                          |
| CD4 <sup>+</sup> T cell | Human          | Mouse mc MT 310            | Biotin          | Streptavidin-peroxidase         | Dako                          |
| CD4 <sup>+</sup> T cell | Human          | Mouse mc Q 4120            | na              | Rabbit-anti-mouse peroxidase    | Dako                          |
| CD4 <sup>+</sup> T cell | Human          | Mouse mc T4                | na              | Rabbit-anti-mouse peroxidase    | Dako                          |
| CD8 <sup>+</sup> T cell | Human          | Mouse mc RFT8              | na              | Goat-anti-mouse IgM phosphatase | Professor G. Janosy           |
| IgG                     | Human          | Rabbit F(ab') <sub>2</sub> | na              | Swine-anti-rabbit peroxidase    | Dako                          |
| IgA                     | Human          | Rabbit F(ab') <sub>2</sub> | na              | Swine-anti-rabbit peroxidase    | Dako                          |
| IgM                     | Human          | Rabbit F(ab') <sub>2</sub> | na              | Swine-anti-rabbit peroxidase    | Dako                          |
| γδ T cell               | Human          | Mouse mc5 A6.E9            | na              | Rabbit-anti-mouse biotin        | Serotec                       |
| HLA-DR                  | Human          | Mouse mc                   | na              | Rabbit-anti-mouse peroxidase    | Dako                          |
| MBP                     | Human          | Mouse mc Clone 10          | na              | Rabbit-anti-mouse biotin        | Groom <i>et al.</i> (1985)    |
| Oligodendrocyte         | Human          | Mouse mc 14E               | na              | Rabbit-anti-mouse biotin        | Newcombe and Cuzner (1988)    |

HLA-DR = human lymphocyte antigen-DR; MBP = myelin basic protein; FITC = fluorescein isothiocyanate; TRITC = tetra-rhodamine isothiocyanate.